





Water Resources Research®

RESEARCH ARTICLE

10.1029/2023WR035594

Fully Developed Open Channel Flow Over Clusters of Freshwater Mussels Partially Buried in a Gravel Bed

T. Lazzarin¹ , G. Constantinescu² , H. Wu² , and D. P. Viero¹ 

¹Department of Civil, Environmental and Architectural Engineering, University of Padova, Padua, Italy, ²Department of Civil and Environmental Engineering and IIHR-Hydroscience and Engineering, University of Iowa, Iowa City, IA, USA

Key Points:

- Mussel-to-mussel interactions are important for dense arrays and influence flow structure and turbulence
- Eddy resolving simulations showed that the effect of bed roughness become less significant with increasing mussel bed density
- In dense clusters of mussels, forces on the shells and bed shear stresses are reduced thus favoring mussel stability

Correspondence to:

T. Lazzarin,
tommaso.lazzarin@unipd.it

Citation:

Lazzarin, T., Constantinescu, G., Wu, H., & Viero, D. P. (2024). Fully developed open channel flow over clusters of freshwater mussels partially buried in a gravel bed. *Water Resources Research*, 60, e2023WR035594. <https://doi.org/10.1029/2023WR035594>

Received 16 JUN 2023

Accepted 9 JUL 2024

Author Contributions:

Conceptualization: T. Lazzarin,

G. Constantinescu, D. P. Viero

Formal analysis: T. Lazzarin

Funding acquisition: D. P. Viero

Investigation: T. Lazzarin

Methodology: T. Lazzarin,

G. Constantinescu, H. Wu

Project administration: D. P. Viero

Supervision: G. Constantinescu,

D. P. Viero

Visualization: T. Lazzarin

Writing – original draft: T. Lazzarin

Writing – review & editing:

G. Constantinescu, D. P. Viero

© 2024. The Author(s). *Water Resources Research* published by Wiley Periodicals LLC on behalf of American Geophysical Union.

This is an open access article under the terms of the [Creative Commons Attribution License](https://creativecommons.org/licenses/by/4.0/), which permits use, distribution and reproduction in any medium, provided the original work is properly cited.

Abstract The present study uses results of eddy-resolving numerical simulations to investigate the open channel flow over large clusters of freshwater mussels (*Unio elongatulus*) partially buried in a rough, gravel bed. The density of the mussels forming the array varies from 26 to 500 mussels/m². The flow structure is analyzed at large distances from the leading edge of the mussel bed, where the flow can be considered fully developed. The effects of changing the mussel bed density, the filtering discharge, the burial level and the roughness of the bed surface in which mussels are burrowed, are investigated in terms of flow field, turbulent structures, drag forces, and bed shear stresses. It is found that strong interactions occur between energetic eddies generated by the larger gravels on the exposed bed surface and by the mussel shells. Simulations results show that for a burial depth close to 50% and a ratio between the average gravel size and the mussel protruding height of 0.13, the shell induced turbulence becomes dominant for mussel bed densities around 50 mussels/m². The influence of the bed roughness becomes less relevant with increasing mussel density, as the generation of energetic eddies is mostly controlled by mussel-to-mussel interactions. For fixed bed roughness, burial level and filtering velocity, the mean streamwise drag force and the associated drag coefficient for the exposed part of each mussel decrease with increasing mussel density, even if strong variations are observed for individual mussels. For constant mussel bed density and burial level, the mean streamwise drag force and the mean drag coefficient decrease slightly with increasing bed roughness. Increasing the burial level decreases not only the drag forces but also the drag coefficients because of the more streamlined shape of the top of the mussels. Strong active filtering acts toward decreasing the mean streamwise force and the mean drag coefficient. The spanwise drag forces contribute significantly to the total drag force, especially for high mussel bed densities. Based on smooth bed calculations, bed-averaged shear stresses are reduced in highly dense clusters.

1. Introduction

Freshwater mussels are found at the water-sediment interface and are considered ecosystem engineers in river environments, as they contribute to filter water, enhance the stability of the bed, provide habitat for other aquatic species, constitute a vital link in the food chain, and are useful bioindicators to detect environmental disturbances (Atkinson & Vaughn, 2015; Gutiérrez et al., 2003; Hajisafarali et al., 2022; Howard & Cufey, 2006; Kreeger et al., 2018; Modesto et al., 2023; Pilbala et al., 2024; Polvi & Sarneel, 2018; Vaughn, 2018; Vaughn et al., 2004).

These mussels have a shell composed of two valves that are slightly asymmetric with respect to a central axis. The shell can open during the filtering process, with an incurrent and an excurrent siphon protruding outwards. Nutrients are acquired through the incurrent siphon, while a jet of clean, filtered water is ejected through the excurrent siphon. Mussels are usually partially buried in the substrate (Vaughn et al., 2008). A muscular foot located in the lower part of the shell allows for small movements in response to external inputs. Live mussels change their direction such that they generally orient themselves parallel to the water flow. Though many factors influence the mussel orientation, the alignment with the incoming flow allows to minimize the total drag force and the probability of being dislocated from the substrate (Di Maio & Corkum, 1997; Wu & Constantinescu, 2022). Observations from real freshwater environments also reveal that siphons generally face upstream, with the exhalant siphon located downstream of the inhalant siphon to maximize the nutrient intake (Di Maio & Corkum, 1997; Perles et al., 2003).

In many part of the world, freshwater mussels represent the dominant benthic invertebrates (Allen & Vaughn, 2009; Strayer, 2008). However, they are also among the world's most imperiled fauna (Ferreira-Rodríguez et al., 2019; Froufe et al., 2017; Lopes-Lima et al., 2017; Lopez et al., 2022; Simeone et al., 2021). As the survival of mussels also depends on flow hydrodynamics, understanding the interactions among the molluscs

and the flow is of great importance for their conservation (Lopez & Vaughn, 2021; Sullivan & Woolnough, 2021; Zigler et al., 2008). A better understanding of the mechanisms and factors that significantly affect the life of mussels (e.g., in terms of stability, availability of nutrients and food) should provide new perspectives on possible actions to be pursued to ensure their survival in natural streams (Nikora, 2010).

Besides laboratory experiments (e.g., Crimaldi et al., 2007; Kumar et al., 2019; Sansom et al., 2020), the physical interactions of mussels with the near-bed flow have been investigated computationally in some recent studies using numerical approaches that resolve the energetically important turbulent eddies in the flow. Flow and turbulent structures, drag forces, sediment entrainment mechanisms leading to local scour and mixing between the excurrent siphon jet of filtered water and the overflow rich in phytoplankton, were investigated for a single partially burrowed mussel placed on a flat bed by Wu et al. (2020) and for a small cluster of three mussels by Constantinescu et al. (2013). The effect of the angle of attack was discussed by Wu and Constantinescu (2022), while the influence of bed roughness was investigated by Lazzarin, Constantinescu, et al. (2023). All these studies shed light on how the mussel interacts with the flow at the organism level, but they were limited to isolated specimens, or to small sets of shells with relatively low spatial density.

In natural rivers, mussels typically develop in very large clusters or arrays, known also as mussel beds (Morales et al., 2006; van de Koppel et al., 2008). The positions of the mussels inside the array are generally irregular. However, in most cases, except for mussel beds characterized by clear self-organizing spatial patterns (de Jager et al., 2020; Folkard & Gascoigne, 2009; Liu et al., 2014), which are beyond the scope of the study, the mussel bed can be well characterized by a unique value of the mussel array density (i.e., the number of mussels per unit area). The value of the mussel density strongly depends on average flow and habitat conditions in the river, as well as on species and dimensions of the shells. In the case of mussel beds, the flow and the vortical structures in the vicinity of the shells are likely to have different characteristics compared to the case of an isolated mussel (Sansom et al., 2022). This is because the mussel-to-mussel interactions become important as the mussel array density increases. In the case of mussel beds, mussel-flow interactions are not only a function of the geometry of the protruding part of the shell and of the filtering discharge, but also a function of the position inside the array and of the relative position of each mussel with respect to the neighboring mussels. The presence of an array of mussels also affects the drag forces acting on the protruding parts of the shells compared to the case of an isolated mussel. Because in large communities mussels are partially sheltered by upstream mussels, the drag forces are expected to decrease with increasing mussel density.

Previous studies on flow over a mussel bed mainly consist of laboratory and field experiments. Earlier studies focused on characterizing the phytoplankton distribution within the boundary layer (e.g., Butman et al., 1994; O'Riordan et al., 1995). Nikora et al. (2002) measured velocity and turbulence profiles in the internal boundary layer over a patch of horse mussels in a tidal environment. Crimaldi et al. (2002) performed measurements in a flume containing model clams at the channel bed. Experiments were performed with different population densities. They concluded that spacing between the clams strongly affects the capability of the clams to remain anchored into the substrate. van Duren et al. (2006) performed flume experiments with living mussels to assess the effects of the mussel filtering activity on the structure of the rough-bed boundary layer induced by the shells. The filtering effect has been shown to play an important role if the excurrent flow velocity was comparable or higher than the mean velocity of the incoming flow. Crimaldi et al. (2007) also evaluated the effect of the filtering activity on the velocity and concentration profiles using idealized models of clams. Sansom et al. (2020) used Particle Image Velocimetry to characterize flow over a gravel bed containing a long array of partially burrowed freshwater mussels. The geometry of the model mussels in their experiments was realistic but did not consider the effect of active filtering. The mussel array density was varied between 0 mussels/m² and 100 mussels/m². They observed a change in flow regime for mussel array densities above 25 mussels/m², with reduced flow velocity and bed shear stresses. Meanwhile, they observed that the largest turbulent shear stresses were located away from the bed, around the top of the protruding mussels.

The present work uses a numerical approach based on Detached Eddy Simulations (DES), similar to that used to investigate flow past a single, isolated mussel partially buried in a rough (gravel) bed (Lazzarin, Constantinescu, et al., 2023) to study flow structure over a long array of partially buried mussels placed at the bottom of an open channel at large distances from the leading edge of the array, where the flow can be considered to be close to fully developed. The interest in studying the fully developed flow regime is motivated by the fact that mussel beds in natural rivers extend over several kilometers. In open channels, as the flow approaches the leading edge of the

mussel bed, an internal boundary layer is generated (Nikora et al., 2002) which eventually reaches the free surface, given the finite flow depth. Some distance downstream, the flow will reach a new “fully developed” state that is independent of the characteristics of the open channel flow approaching the mussel bed (e.g., fully developed flow over a gravel bed containing no mussels). This new, fully developed state will be observed until the end of the mussel bed. Reproductions of a real gravel bed surface are used in the rough-bed simulations. The shape of the shells accurately reproduces that of an *unionid* mussel and the numerical model includes the filtering flows through the excurrent and incurrent siphons.

Compared to previous flume experiments conducted with freshwater mussels, the present study investigates the effect of the mussel array density up to large values corresponding to highly dense mussel beds. Average mussel bed densities for mussels of similar species and dimensions ranges from 0 to 100 mussels/m² (Coco et al., 2006; Sansom et al., 2018, 2020), but mussel beds of higher densities are sometimes observed in rivers (Miller & Payne, 1988; Steuer et al., 2008; Strayer et al., 1994). Mussel bed densities in rivers can reach values of about 500 mussels/m² (e.g., though for different species, 380 mussels/m² in André et al., 1993, and 625 mussels/m² in O’Riordan et al., 1995). Thus, the value of 500 mussels/m² is chosen as an upper threshold in the present study. A main advantage of the present numerical approach that resolves the flow past the individual mussels is that it allows investigating the near-bed flow beneath the top of the mussels. Performing measurements in this region is very complicated especially at high mussel array densities due to the very small spacing between the mussels. A main aim of the present study is to better understand how the interactions between the turbulent eddies generated by the rough bed and the protruding parts of the mussels, and the wake-to-mussel interactions affect the flow structure, the destabilizing drag forces acting on the mussels and the bed shear stresses.

The paper is organized as follows. Section 2 introduces the test cases and the numerical model used in the present analysis. Section 3 describes the flow turbulence structure in the open channel and the coherent structures generated by the protruding parts of the mussels. Section 4 discusses the effects of the controlling parameters on the drag forces acting on the mussels, while Section 5 describes the bed shear stress distribution. Finally, conclusions are included in Section 6.

2. Materials and Methods

2.1. Test Cases

The mussel model used in the numerical simulations was based on a 3-D reproduction of a real specimen of a dead *Unio elongatulus* mussel (Termini et al., 2023), popular in Italian freshwater environments (Marrone et al., 2019; Modesto et al., 2023). In each simulation, the mussels were aligned with the incoming flow. The major axis of each mussel was inclined toward upstream in a streamwise-vertical plane. The total length of the shell was 0.08 m; the other geometrical dimensions, projected along the x , y , z axes, were the mussel length $L = 0.055$ m, width $b = 0.020$ m and height $H = 0.050$ m (Figure 1a). Most of the simulations were conducted with a mussel burial level of $h/H = 0.48$ (h is the height of the exposed part of the shell). Two simulations were conducted with $h/H = 0.28$ to investigate the effect of the burial level on the flow. For each simulation, the burial level was the same for all the mussels in the array and the exposed height, h , served as the reference length-scale for the roughness height of the mussel bed.

The simulations were performed in a rectangular straight open channel, 0.5 m ($10 H$) wide and 1.0 m ($20 H$) long (Figure 1b), that is, much larger than the largest coherent structures having a length of $\sim 6 h$ ($3 H$) for burial level of $h/H = 0.48$ (see also Lazzarin, Constantinescu, et al., 2023 for cases with isolated mussels). The bed surface was 0.5 m^2 , and the water depth $D = 0.15$ m ($3 H$). The flow rate through the channel was $Q = 0.0123 \text{ m}^3/\text{s}$, and the section-averaged, or bulk, velocity was $U_0 = 0.164 \text{ m/s}$. The Froude number was 0.14, the bulk Reynolds number 24,600. This simulated scenario is similar to the laboratory conditions used to investigate freshwater mussel’s behavioral response as part of the same project (e.g., Modesto et al., 2023; Termini et al., 2023). Those laboratory conditions were determined based on those in a natural stream in Italy where such mussels are encountered. Thus, the hydrodynamic set-up used in the present study represents a realistic habitat for the mussels.

The main physical parameters investigated in the present study are the mussel array density, ρ_M , the ratio between the bed roughness height and the protruding height of the mussel, d_{50}/h , the filtering velocity ratio, VR (i.e., the

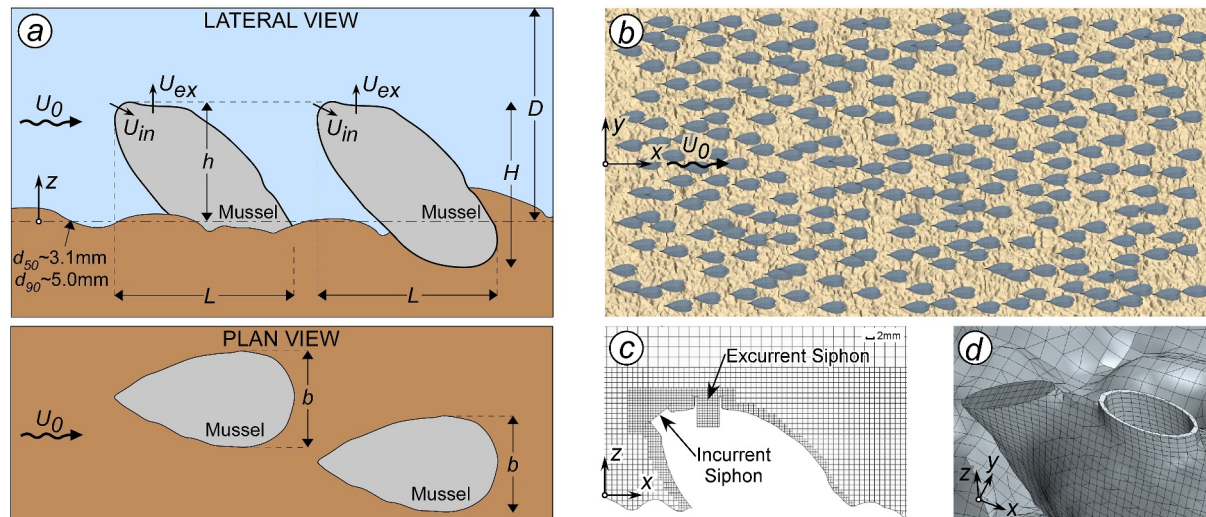


Figure 1. (a) Sketch showing two of the shells part of the mussel bed. U_0 is the section-averaged velocity in the channel, L , H , and b are the mussel length, height and width in the x , y , z reference frame, respectively ($z = 0$ identifies the mean bed elevation), h is the height of the exposed part of the mussel, U_{in} and U_{ex} are the mean velocities through the incurrent and the excurrent siphons, respectively, and D is the height of the water column above the bed; (b) plan view showing the mussel bed with $\rho_M = 500$ mussels/m²; (c) longitudinal section showing the mesh around a mussel shell; (d) 3-D view of the computational domain with the surface mesh around the region containing the two siphons.

ratio between the excurrent jet velocity, U_{ex} , and the bulk velocity in the channel, U_0 , and the burial level, h/H . The main characteristics of the test cases described in the present paper are included in Table 1.

Most of the simulations were performed over a rough-bed with $d_{50} = 3.10$ mm and $d_{90} = 5.00$ mm, which reproduced a water-worked gravel bed sample from a previous laboratory experiment. More details are provided in Section 2.2 and in Lazzarin, Constantinescu, et al. (2023). In the simulations with no mussels, the roughness Reynolds number was 210. Some simulations were performed over a flat bed ($d_{50} = 0.00$ mm), while others were performed over a gravel bed obtained by multiplying the vertical coordinate of the original gravel bed by a factor of 0.5. In this last case, we estimated $d_{50} = 2.46$ mm. The value of d_{50} is used as length-scale of the roughness height of the gravels.

Simulations were performed considering clusters of different densities, spanning from 26 mussels/m² to 500 mussels/m², which correspond to a total number of mussels within the computational domain ranging between 13 and 250. An additional simulation was performed with a rough bed and no mussels (0 mussels/m²) to allow comparing with the case of fully developed open channel flow over a gravel bed.

The study also considered different filtering discharges through the two siphons of the mussels. The volumetric flux rates through the inhaling and the exhaling siphons were equal to each other ($Q_{in} = Q_{ex}$) and constant in time to mimic a continuous jet (Nishizaki & Ackerman, 2017). This aligns with previous experiments (e.g., Monismith et al., 1990; Sansom et al., 2018) and represents a realistic assumption given that variations in filtering discharge generally occur over longer time scales compared to the time span investigated. For each simulation, these two discharges were identical for all mussels forming the array. Simulations were performed with filtering discharges of $3.3 \cdot 10^{-8}$, $1.3 \cdot 10^{-6}$, and $3.1 \cdot 10^{-6}$ m³/s, which are within the range expected for mussels of similar species and dimensions (Bunt et al., 1993; Kryger & Riisgård, 1988; Monismith et al., 1990; Riisgård et al., 2011). The corresponding values of the velocity ratio, $VR = U_{ex}/U_0$, are 0, 0.5, and 1.22. The intermediate value corresponds to an average filtering condition given the species and the dimension of the mussel considered in the study.

2.2. Computational Model

The simulations were performed using the viscous flow solver in STAR-CCM+, widely used to simulate complex flows in natural environments (Constantinescu, 2014; Keylock et al., 2012; Lazzarin, Viero, et al., 2023). The model adopted in the present study was the same as the one used by Lazzarin, Constantinescu, et al. (2023) to

Table 1
Matrix of Simulations With Relevant Parameters

N	ρ_M	d_{50}/h	d_{50}/H	VR	h/H	U_{inner}/U_0
0	0	0.13	0.062	–	0.48	–
13	26	0.13	0.062	0.50	0.48	0.587
50	100	0.13	0.062	0.50	0.48	0.557
100	200	0.13	0.062	0.50	0.48	0.519
150	300	0.13	0.062	0.50	0.48	0.426
200	400	0.13	0.062	0.50	0.48	0.387
250	500	0.13	0.062	0.50	0.48	0.348
50	100	0.00	0.000	0.50	0.48	0.627
100	200	0.10	0.049	0.50	0.48	0.530
100	200	0.00	0.000	0.50	0.48	0.553
250	500	0.10	0.049	0.50	0.48	0.372
250	500	0.00	0.000	0.50	0.48	0.390
100	200	0.13	0.062	0.00	0.48	0.483
100	200	0.13	0.062	1.22	0.48	0.501
250	500	0.13	0.062	0.00	0.48	0.353
250	500	0.13	0.062	1.22	0.48	0.392
50	100	0.00	0.000	0.50	0.28	0.445
50	100	0.22	0.062	0.50	0.28	0.575

Note. N is the number of mussels in the computational domain, ρ_M is the mussel array density, h is the emerged height of the mussel, H is the total height of the mussel, d_{50} is the median diameter of the channel bed material, $VR = U_{ex}U_0$ is the filtering velocity ratio, U_0 is the section-averaged, or bulk, velocity, U_{inner} is the mean streamwise velocity in the region $z < h$.

which the reader is referred for a complete description of the numerical methodology. Some relevant aspects are described below.

The Detached Eddy Simulation (DES) hybrid approach was used in the present study. It reduces to Large Eddy Simulations (LES) away from the solid surfaces and to Reynolds-Averaged Navier-Stokes (RANS) turbulence model near solid boundaries (Constantinescu et al., 2003; Heinz, 2020; Menter et al., 2021). The turbulent scale in the LES region is defined based on the local grid spacing, like in the classical LES. By contrast, the turbulence length scale is proportional to the distance to the closest solid boundary in the RANS region. In the present application, the Shear Stress Transport $k-\omega$ model (Menter, 1994; Menter et al., 2003) was used as the base RANS model. Similar to the previous DES investigations of flow past mussels (Lazzarin, Constantinescu, et al., 2023; Wu et al., 2020), the viscous sublayer was fully resolved to avoid the introduction of wall functions (the first grid point off the solid surface in the wall normal direction is at 5–7 wall units). This kind of model has been shown to provide accurate results for open channel flows and flow in natural river reaches (Constantinescu, 2014; Keylock et al., 2012). DES was successfully used to study the physics of open channel flows containing large arrays of surface-mounted emerged and submerged obstacles (e.g., Chang et al., 2017, 2020; Koken & Constantinescu, 2020) and open channel flows with large-scale roughness elements in the form of an array of 2-D dunes (Chang & Constantinescu, 2013).

The finite volume method was used to integrate the Navier-Stokes equations on unstructured Cartesian-like grids with the SIMPLE algorithm (Patankar & Spalding, 1972). Convection terms were discretized with a Hybrid-Bounded central difference scheme, while a second-order upwind scheme was used for the convective terms in the transport equations solved for the eddy viscosity. The diffusive and pressure gradient terms were solved using a second-order central scheme.

No-slip boundary conditions were applied on the bed surface and on the mussel shells. A mass outlet boundary condition was applied at the incurrent siphon, and a mass flow inlet boundary condition was imposed at the entrance section of the excurrent siphon pipe (Figure 1c). The standard procedure to determine the values of the turbulent variables at the solid surfaces was used (Menter, 1994). Considering the low value of the Froude number (0.14) and high submergence $D/h > 4$, the deformations of the free-surface are expected to produce negligible effects on the flow field close to the mussel bed (Hajimirzaie et al., 2012; Koken & Constantinescu, 2009; Shamloo et al., 2001); hence, the use of the rigid lid approximation at the top boundary is justified in the present simulations. Periodic boundary conditions were imposed in both the streamwise and spanwise directions for flow velocity and turbulence model variables.

The present numerical model shares the same setup (e.g., mussel species, rough bed surface) as the one used by Lazzarin, Constantinescu, et al. (2023), which was validated using data from laboratory experiments for flow past an isolated mussel placed on a rough bed. An additional validation analysis of the computational approach is discussed in Wu et al. (2020).

The computational domain has been set up using the STAR-CCM+ mesh generator. The gravel bed surface and the mussel shell surface were digitized from separate data files. Their surfaces were imported in STAR-CCM+ as stereolithography files containing triangular meshes. Using symmetry projections, the original grained bed surface was used to generate a larger bed surface such that the bed elevation was identical at the upstream and at the downstream edges of the mesh, and also at its right and left sides. This was needed to impose periodic boundary conditions at those pairs of boundaries. Two additional parts have been added to the shell geometry to mimic the presence of the incurrent and the excurrent siphons of the mussel, as detailed in Lazzarin, Constantinescu, et al. (2023) (Figures 1c and 1d). The positions of the mussels in the array have been determined using a randomization procedure, following what was done in the flume study of Sansom et al. (2020). Additional constraints have been introduced to ensure a nearly uniform mussel density in the whole domain (i.e., to avoid

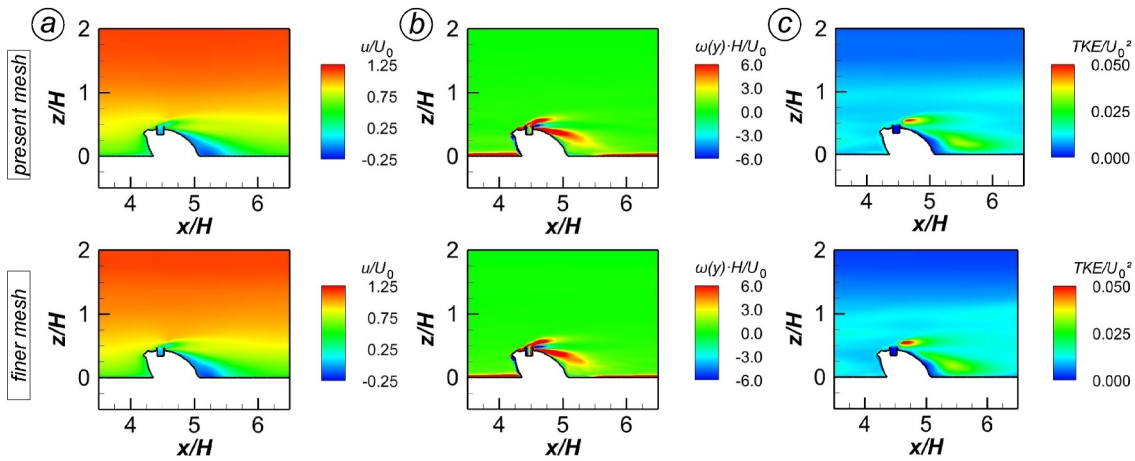


Figure 2. Mesh sensitivity analysis: mean velocity, w/U_0 (a), mean spanwise vorticity, $\omega_y H/U_0$ (b), and turbulent kinetic energy, TKE/U_0^2 (c) in a longitudinal section crossing a mussel in coarser (top line) and finer (bottom line) mesh simulations of flow over an array of mussels. The simulations were conducted for $\rho_M = 100$ mussels/ m^2 , $d_{50}/h = 0.0$, $VR = 0.50$ and $h/H = 0.48$.

spatial aggregations in some part of the channel) and a minimum distance between neighboring mussels (i.e., to avoid overlapping among the shells). The mussel shell surface with siphons was copied and placed over rough or smooth bed surfaces centered at the x, y coordinate couples provided by the randomization procedure. The burial level was set close to 50%, such that $h/H = 0.48$ (Figure 1a), or to 75% (in this case $h/H = 0.28$), and the mussel parts beneath the bottom was removed to obtain the final mesh.

The computational grid, in terms of mesh refinement, minimum distance to the solid surfaces, and average size of the cells in different regions, fulfilled the same criteria as those described in Lazzarin, Constantinescu, et al. (2023), to which the reader is referred for additional details. The mesh is progressively refined close the bed and around the emerged part of the mussels. The mean cell dimension decreased from 0.0048 m (≈ 56 wall units) in the upper part of the domain to 0.0012 m (≈ 14 wall units) in the near-bed region containing the bed surface and the protruding mussels (Figure 1c). The regions surrounding the siphons were meshed with a resolution of 0.0005 m (≈ 6 wall units). The total number of cells used to mesh the computational domain in the various simulations was close to 13 million.

The level of mesh refinement around each mussel is basically the same as the one used by Lazzarin, Constantinescu et al. (2023) in their study of a single mussel placed on a gravel bed. This level of grid density was shown to produce grid independent solutions based on sensitivity analysis performed for the case of a single mussel placed on a gravel bed (see Lazzarin, Constantinescu et al., 2023). As the flow around isolated mussels is different from flow past arrays of mussels where strong mussel-to-mussel interactions may be present, we also verified that the meshes used in simulations with arrays of mussels were fine enough to ensure mesh independent solutions. Flow over an array of mussels was simulated in a reduced domain containing 9 mussels where the distance between the mussels was sufficiently low for strong mussel-to-mussel interactions to occur (e.g., $\rho_M = 100$ mussels/ m^2). Two simulations have been performed: one with the same level of mesh refinement as used for the simulations listed in Table 1 (i.e., same as in Lazzarin, Constantinescu, et al., 2023), and the other with a finer mesh, where the number of computational cells was more than double. These simulations have been conducted with $\rho_M = 100$ mussels/ m^2 , $d_{50}/h = 0.0$, $VR = 0.50$, $h/H = 0.48$. We then compared the two solutions in terms of velocity, vorticity (x, y, z components) and turbulent kinetic energy (TKE) around all mussels forming the array. As also exemplified by the results presented in Figure 2 for one of the mussels in the array, the coarser mesh predictions of the mean flow and turbulence statistics variables were very close to those of the finer-mesh simulation. The predicted drag forces on all the mussels in the computational domain in the two simulations were also very close (less than 3% difference).

By imposing periodic boundary conditions at the upstream and downstream boundaries of the domain, a 1 m-long stretch of an infinitely long channel with periodic bathymetry was simulated in the simulations reported in Table 1. Simulations were run until the velocity components became statistically steady in the mean. Results were analyzed over a subsequent 20 s long time interval, which corresponds to about 3.3 flow-through time periods

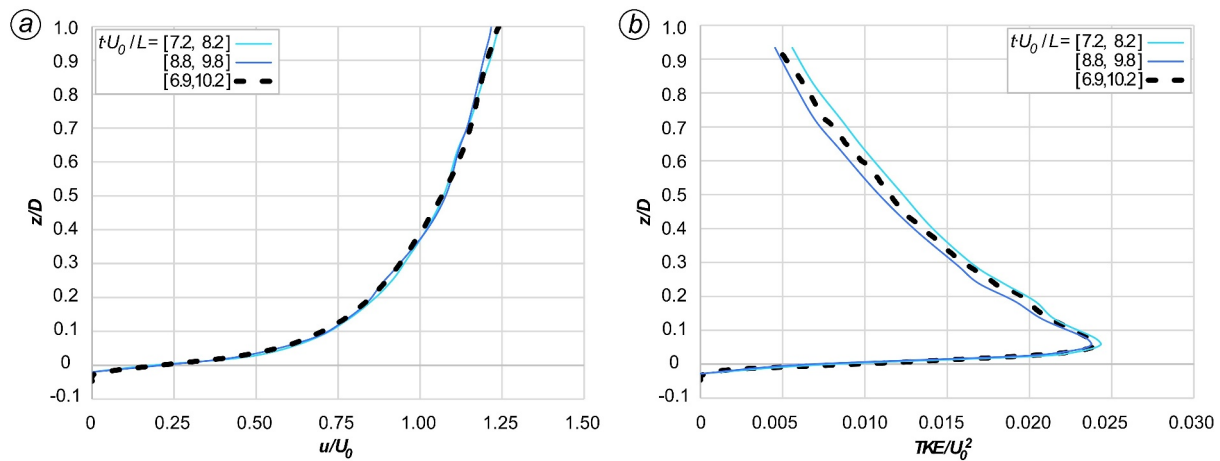


Figure 3. Convergence of mean flow and turbulence statistics: vertical profiles of the double-averaged mean velocity, u/U_0 (a), and turbulent kinetic energy, TKE/U_0^2 (b). Thin, solid lines show results averaged over a $1.0 L/U_0$ long time interval; thick, dashed lines show results averaged over a $3.3 L/U_0$ long time interval. Results are plotted for the simulation conducted with $\rho_M = 25 \text{ mus/m}^2$, $d_{50}/h = 0.13$, $VR = 0.5$, and $h/H = 0.48$.

over the 1 m stretch. To ensure that the flow has reached time-invariance over the entire flow depth, we analyzed the time series of velocity (at different depths and locations) and the double-averaged profiles over the width and length of the domain of the mean longitudinal velocity and TKE , by time-averaging these variables over different time windows. Results reported in Figure 3 show that the profiles computed in $1.0 L/U_0$ -long time intervals are close to those computed over the $3.3 L/U_0$ -long time interval which is the time interval used for calculating the statistics reported in the results sections. The mean flow computed in the periodic domain corresponds to a fully developed flow solution that will be reached in a very long open channel at very large distances from the leading edge of the mussel bed. This regime is particularly important, given that mussel beds generally extend over very distances of the order of kilometers in rivers.

3. Fully Developed Turbulent Flow Over a Mussel Bed

3.1. Effects of Overflow and Bed Roughness on the Protruding Mussels

Flow over an isolated mussel can be considered a particular type of flow past a surface-mounted obstacle, further complicated by the irregular shape of the shell and by the filtering activity of the mollusk. In a cluster of mussels, the presence of neighboring shells produces additional turbulent structures and deviates the incoming velocity, making the flow field approaching each shell more complex. For both an isolated specimen and a cluster of mussels, the picture is even more multifaceted when considering a rough bed instead of a smooth one, since gravel particles are an additional source of turbulence. For the case of a dense array of mussels ($\rho_M = 500 \text{ mussels/m}^2$), Figure 4 shows the mean pressure on mussel shells and at the bed for simulations with smooth (a) and rough (b) beds. The mean pressure distribution on the protruding parts of the shells shows an overall decay of the pressure along the streamwise direction due to the drag and head losses induced by the mussel bed, which is coherent with what is expected to be observed in an open channel flow over a smooth or a rough bed (see Section 2.2). The mean pressure gradient increases with the overall roughness of the bed surface that includes the effects of the gravel particles and/or protruding mussels. For both the smooth and the rough bed cases, the highest-pressure values are observed over the frontal part of the shell, immediately below the incident siphon. Here, the flow is decelerated and deviated laterally by the mussel shell, similar to the flow around any surface-mounted obstacle. The lowest pressure values are observed just downstream of the excurrent siphon, over the upper part of the shell. Although this qualitative trend is observed for all the shells, regardless of the mussel density, notable variations in the mean pressure values at the front and back of the shells are observed depending on the position of the mussel in the array, especially for denser clusters (e.g., compare mussels pointed out by the arrows in Figure 4a, which have similar x coordinates).

Mussels subjected to higher pressure forces may be displaced by the flow with a higher probability (see also quantitative discussion in Section 4 on drag forces), or they can adjust their planimetric position and/or burial level. Thus, mussels can migrate or be dislocated by the flow and this, in turn, may control the arrangement of the

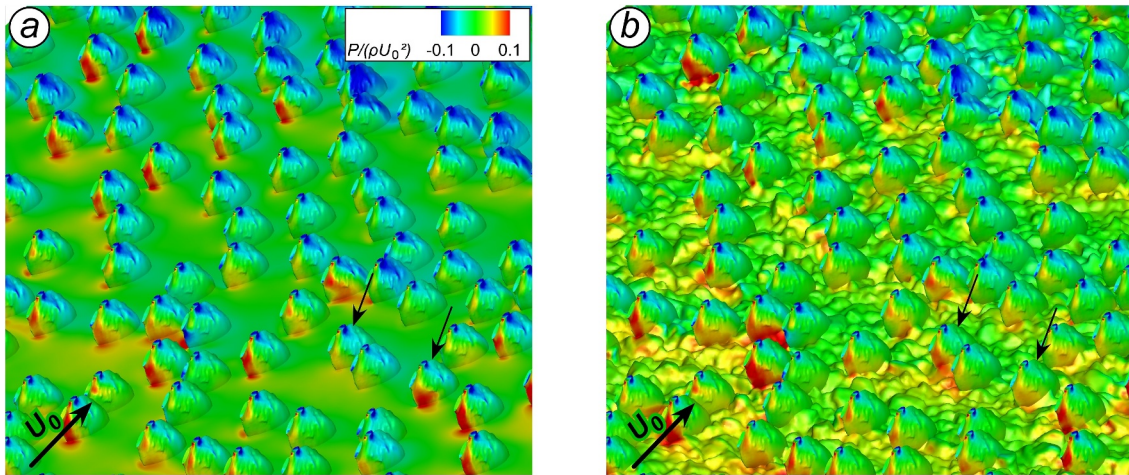


Figure 4. Mean pressure, $P/(\rho U_0^2)$, on shells and bed for simulations with $\rho_M = 500$ mussels/m², $VR = 0.50$, $h/H = 0.48$ for (a) a smooth bed ($d_{50}/h = 0.00$), and (b) a gravel bed ($d_{50}/h = 0.13$).

mussels and the mussel bed density. Among the different factors that concur to modify the pressure distribution on the shells, the relative position in the array is one of the most important because of either sheltering or acceleration of the incoming flow relative to the shell by the neighboring mussels. The pressure on mussel shells also depends on the bed roughness, because the irregular gravel distribution can substantially contribute in modifying the local flow field (e.g., compare mussels pointed by arrows in Figures 4a and 4b).

The presence of sufficiently strong adverse pressure gradient at the front of the mussel may generate a horseshoe vortex around the junction line between the mussel and the bed (Constantinescu et al., 2013; Wu et al., 2020). Analysis of the large-scale coherent structures in the instantaneous and mean flow fields (shown in Figure 5 for $\rho_M = 500$ mussels/m² and $d_{50}/h = 0.13$) reveals no horseshoe vortices form around the upstream base of the mussels, regardless of the array density. Though some small vortex cores were observed in front of the mussels in the rough bed simulations, the comparison with the corresponding flat-bed simulations confirmed that such structures are induced by the gravels. This is in agreement with the findings of Lazzarin, Constantinescu, et al. (2023) for the case of an isolated *Unio elongatulus* mussel (same as the mussel species used in the present study). Wu et al. (2020) observed the formation of horseshoe vortices for an isolated *Lampsilis siliquoidea* mussel placed on a smooth bed. The different behavior can be explained by the vertical inclination of the main axis and by the relatively streamlined shape of the *Unio elongatulus* shell compared to the mussel used in the study of Wu

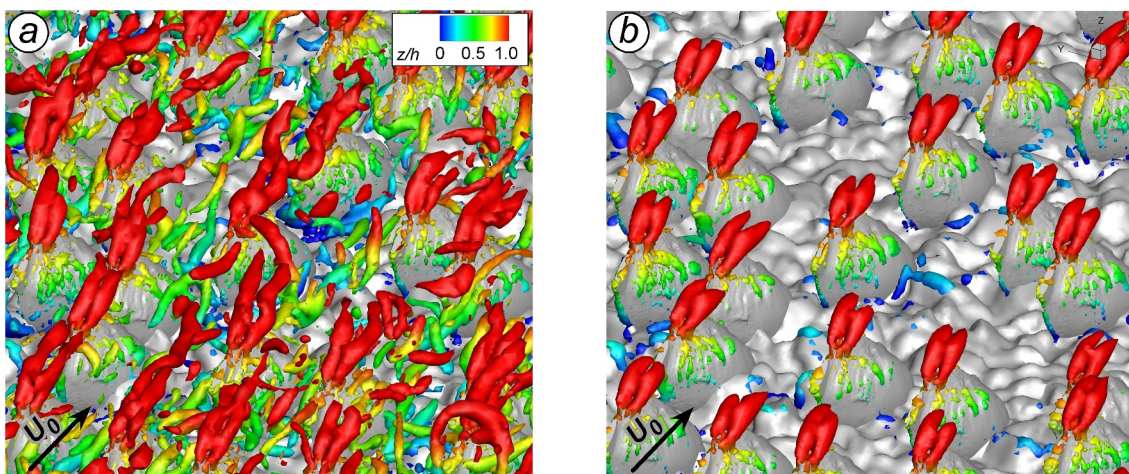


Figure 5. Coherent structures visualized using the Q criterion for the instantaneous (a) and the mean (b) flow in the simulation with $\rho_M = 500$ mussels/m², $d_{50}/h = 0.13$, $VR = 1.22$, $h/H = 0.48$.

et al. (2020). A decrease in the overall degree of bluntness of the surface mounted obstruction is known to weaken and eventually suppress the horseshoe vortices (e.g., Khosronejad et al., 2012). For arrays of mussels with sufficiently large mussel bed density, most of the shells are generally located at least partially in the wake of an upstream shells. The formation of strong adverse pressure gradients in the wakes of the surface-mounted obstacles (e.g., shells in the present simulations) is impeded by the reduction in the velocity magnitude inside the roughness layer. This is consistent with results obtained for arrays of submerged cylinders (e.g., see Chang et al., 2020; Koken & Constantinescu, 2023) that showed horseshoe vortices were suppressed for the surface mounted obstacles situated away from the leading edge of the array. So, for arrays of mussels, the coherence of such vortices, if they form, is expected to be lower and no such vortices will form around most mussels in the array for a sufficiently high mussel bed density.

The turbulent structures in Figure 5 show that pairs of counter-rotating vortices originate downstream of the excurrent siphons in case of active filtering. As observed for an isolated mussel, these vortices are not present for $VR = 0$ and their strength increases with VR . The coherence of these vortices seems quite insensitive to the bed roughness, probably due to the relatively low burrowing ratio considered in the simulations. The vortices are observed in both the instantaneous and mean flow fields in Figure 3. These vortices are also present in the high mussel density simulations (i.e., $\rho_M > 100$ mussels/m²), where jets interfere with each other (Figure 3a). The comparison of different cases showed that the streamwise length of these vortices decays and their coherence reduces with increasing ρ_M due to stronger interactions with energetic eddies generated by the neighboring mussels.

The mussel bed density also influences the distribution of turbulent structures in the roughness layer (i.e., the layer directly influenced by the large-scale roughness, e.g., mussels and gravels, when present). For an isolated mussel, a pair of tip (downwashing) vortices forms in the wake (Lazzarin, Constantinescu, et al., 2023). The coherence of these downwashing vortices is reduced in case of active filtering and especially in case of a rough bed, because of strong interactions between the vortices and the gravel particles. This effect is enhanced in the case of arrays of mussels because mussel-to-mussel interactions contribute to reducing their symmetry, their stretching and ultimately to their loss of coherence. For denser arrays, the formation of these tip vortices downstream the shell is further impeded by the presence of other shells, so that only weak downwashing vortices form and they rapidly lose their coherence. At very high mussel densities, these vortices are basically suppressed for all the mussels forming the array (i.e., they are not observed for $\rho_M = 500$ mussels/m², see Figure 5b).

In general, energetic eddies generated by the bed particles and by the protruding shells are located below the top of the mussels and slightly above them. The trajectories of the larger-scale structures are affected by the shells of the downstream mussels. The region situated immediately above the bed generally contains only small coherent structures in cases with a high mussel density even if the bed is rough. This contrasts with what is observed in the corresponding gravel bed simulation without mussels, in which larger bed particles are found to generate fairly larger, energetic coherent structures above the bed. This effect is expected to reduce the influence of the bed roughness in case of dense clusters and also to reduce the erosive potential of the flow.

The interactions of energetic eddies generated by the largest exposed gravels with the shells are visualized in Figure 6, which shows the spanwise vorticity distributions in an instantaneous flow field in the $z/H \leq 2$ region. For a gravel bed without mussels, the regions of high vorticity are generally situated very close to the bed (Figure 6a). For most of the larger bed particles that penetrate significantly above the average bed elevation (e.g., $x/H = 8.25$), flow detachment is observed, with vorticity sheets above the top of these elements and small separated regions downstream. A high-vorticity region covers the top of the deformed bed, and eddies rarely extend above $z/H > 0.5$. By contrast, arrays of mussels generate more turbulent eddies and modify the flow in the lower part of the water column (Figure 6b) by decreasing the flow velocity and reducing the vorticity at the bottom, especially in regions where mussels are close to each other. Energetic turbulent eddies generated by the gravel particles and by the shells interact with each other and extend up to $z/H \sim 1$ (Figures 6b–6d).

As observed for an isolated mussel, a separated region forms downstream of each shell, and a sheet of high vorticity is observed starting at the top of the mussel and extending over part of the wake (see e.g., mussels at $x/H = 4.5$ and $x/H = 8.5$ in Figure 6b). For mussels placed on a mussel bed, the vorticity sheet generally has a reduced length compared to the case of an isolated mussel (Lazzarin, Constantinescu, et al., 2023). This can be explained both by the increased mussel-to-mussel interactions and by the velocity reduction within the roughness layer, which increase with ρ_M .

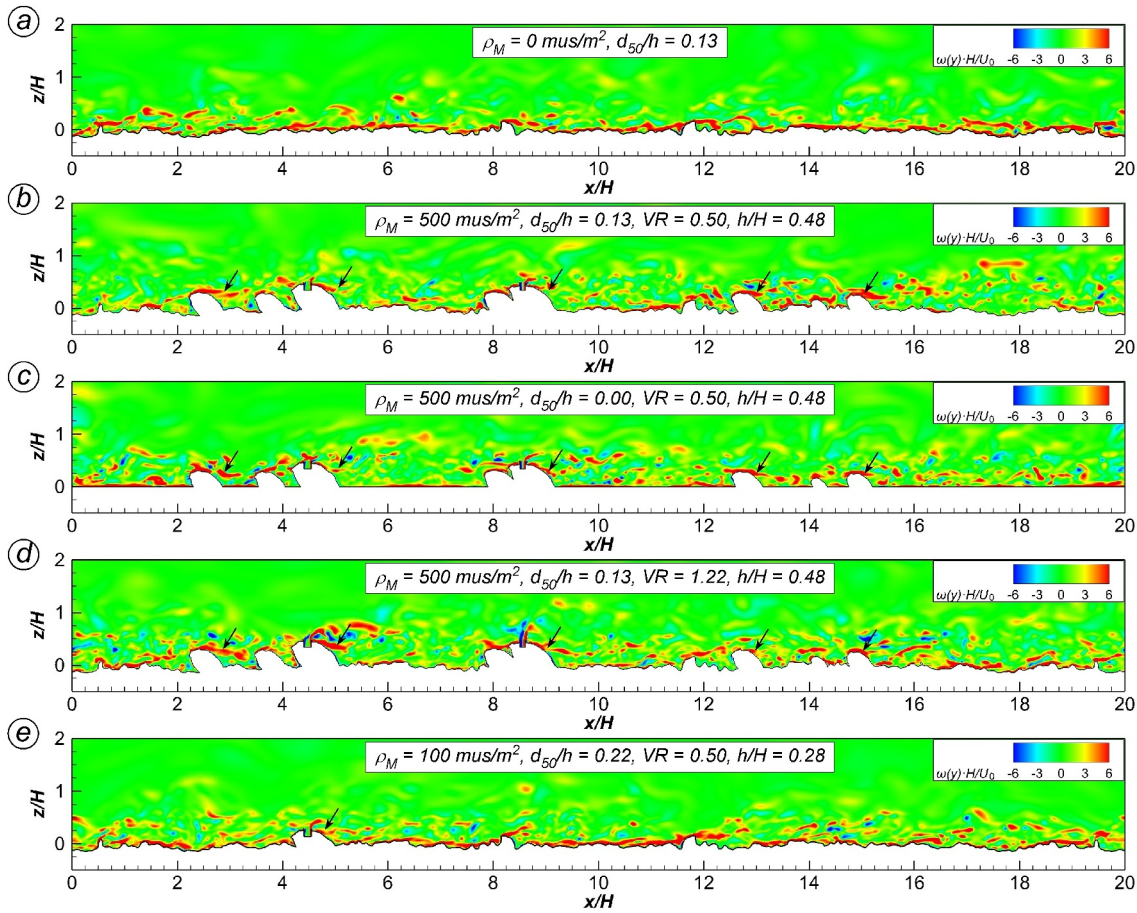


Figure 6. Instantaneous spanwise vorticity, $\omega_y H/U_0$, in the $y/H = -0.7$ plane for different simulations (a–e). Black arrows are pointing toward main shear layers on top of the mussels.

For high-density clusters, a similar vorticity field is observed in simulations conducted with a rough (Figure 6b) and with a smooth bed (Figure 6c), confirming that the gravel roughness plays a role only when/where mussels are sparse. The effect of the active filtering is evident only in relatively small areas situated above the excurrent siphon, where the excurrent siphon jet interacts with the incoming flow (Figure 6d). When increasing the burial level (i.e., decreasing h/H), the mussels' shells behave similarly to the larger bed particles, with a vorticity sheet situated above the top of the shell and a small separation region at its back (e.g., see flow around the mussel situated at $x/H = 4.5$ and flow around larger bed particles around $x/H = 11.8$ and 16.0 in Figure 6e showing instantaneous vorticity field for a simulation performed with $h/H = 0.28$).

3.2. 3-D Effects on the Mean Flow

In simulations conducted with no mussels, the gravel bed particles induce regions with non-negligible mean vertical velocities (e.g., around $x/H = 8$, $y/H = \pm 1$ in Figure 7a). In simulations conducted with mussels, bed-induced upwelling and downwelling regions are confined to the largest mussel-free regions for low mussel densities. Such regions are almost completely suppressed for high mussel densities. Meanwhile, strong upwelling and downwelling flow regions are induced in between the shells (e.g., for $x/H = 7$, $y/H = 2$, and $x/H = 15$, $y/H = 1$ in Figure 7b) because of mussel-to-mussel interactions for high mussel bed densities. The strength of these vertical motions is fairly independent of the bed roughness. Close-to-symmetric regions of flow upwelling are observed to form at the sides of isolated shells (Lazzarin, Constantinescu, et al., 2023). In case of neighboring mussels, these upwelling regions can merge, enforcing the strength of the vertical motions.

Lazzarin, Constantinescu, et al. (2023) identified a region of strong downwelling flow near the symmetry plane of an isolated mussel, which was stronger over a smooth bed and weaker when the active filtering was on and/or in

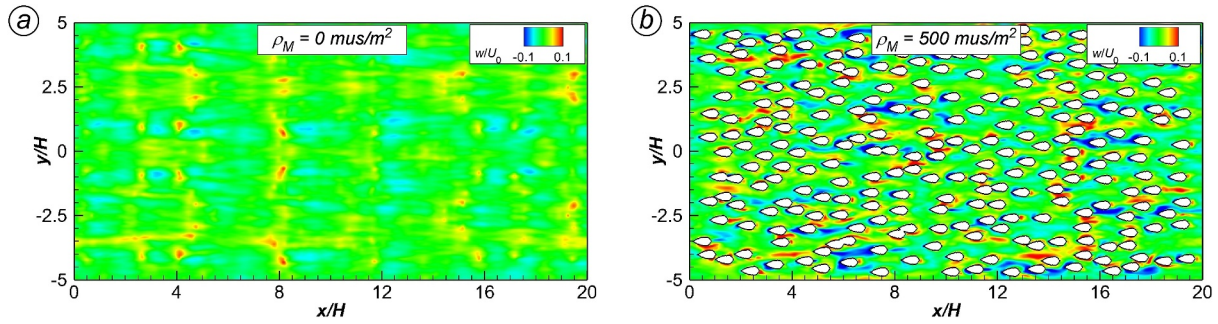


Figure 7. Mean vertical velocity, w/U_0 , for the simulations with $d_{50}/h = 0.13$, $VR = 0.5$, $h/H = 0.48$ and with $\rho_M = 0$ mussels/m² (a) and $\rho_M = 500$ mussels/m² (b), in the horizontal plane with $z/h = 0.5$.

the presence of a rough bed. For mussels part of a mussel bed, the wake interaction with the downstream shells suppresses this downwelling region for many of the mussels in the array (Figure 7b). To quantify the influence of ρ_M , as well as those of the bed roughness and of the filtering activity, the vertical, time-averaged, downward volumetric flux, Q_W , has been evaluated numerically at $z/h = 0.5$:

$$Q_W = \int_{w < -w_t} |w| dA \quad (1)$$

where w is the time-averaged vertical component of flow velocity and $w_t = 0.1 U_0$ is the threshold value chosen to identify regions of strong downwelling motions. One should point out that in the gravel bed simulation conducted with no mussels the largest fluctuations of the vertical velocity are close to $0.1 U_0$.

The results are shown in Figure 8, where Q_W is scaled (left panels) with the average flow rate through a vertical plane of height H and width B , (U_0HB), and also (right panels) with the number of mussels N and the average flow rate through a $H \times H$ vertical plane, (NU_0H^2). $Q_W/(U_0HB)$, and hence the three-dimensionality of the flow, increases with the mussel density (Figure 8a). Figure 6a also shows that $Q_W/(NU_0H^2)$ decreases with ρ_M for low values of the mussel bed density, and attains an almost constant value for $\rho_M > 100$ mussels/m². This means that, beyond a given mussel density, the intensity of the downwelling flow increases only because of the increasing number of mussels, whereas the vertical flow per mussel remains nearly constant inside the mussel bed.

Both $Q_W/(U_0HB)$ and $Q_W/(NU_0H^2)$ decrease with increasing bed roughness (Figure 8b), at a rate that decreases for higher mussel densities. This is consistent with results of Lazzarin, Constantinescu, et al. (2023) who observed stronger downflows for smooth bed conditions. When increasing the bed roughness, turbulence produced by gravel particles destroys the symmetry of tip vortices forming downstream of the mussel, with the downwelling region breaking into multiple asymmetrical subregions of weaker intensity. In the case of denser arrays, the additional turbulence produced by neighboring shells overcomes the bed-induced turbulence, which does not play any significant role.

The filtering activity of the mussel has a fairly negligible effect on Q_W (Figure 8c). Both $Q_W/(U_0HB)$ and $Q_W/(NU_0H^2)$ slightly decrease with increasing VR and then increase for $VR > 0.5$. Moderate filtering further weakens the upwelling and downwelling flow motions, whereas the high velocity of the excurrent jet forming above the top of the mussels for higher values of VR produces stronger coherent structures that enhance the vertical exchange inside the roughness layer.

Figure 8d shows that for constant mussel bed density ($\rho_M = 100$ mussels/m²) and filtering discharge ($VR = 0.5$), Q_W decreases to negligible values as h/H decreases from 0.48 to 0.28. This result is consistent with the observations of Lazzarin, Constantinescu, et al. (2023) for an isolated mussel, who found a strong reduction of the downflow motions with decaying h/H , at least for $h/H > 0.5$.

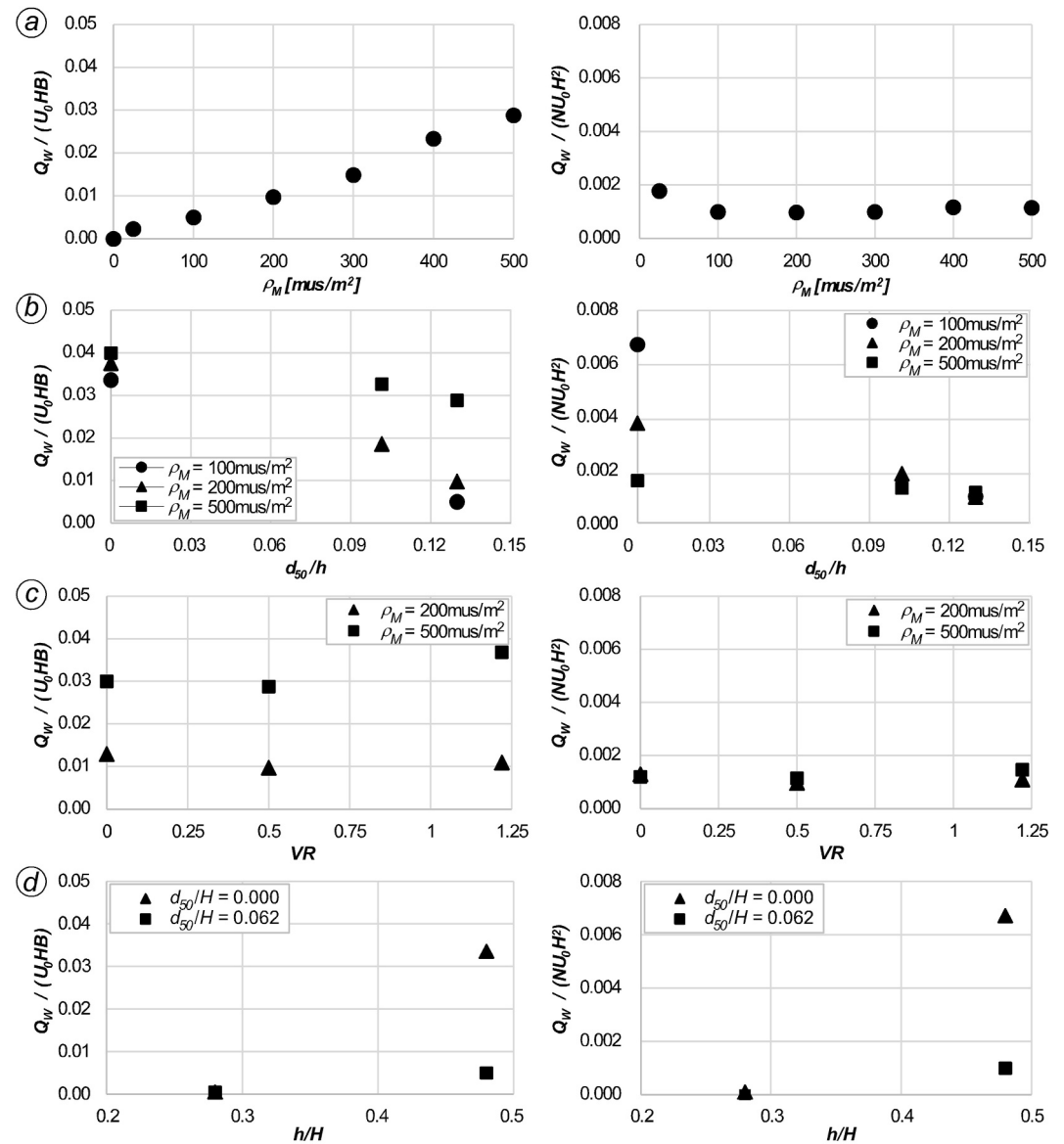


Figure 8. Non-dimensional, time-averaged downward discharge through the $z/h = 0.5$ horizontal plane as a function of (a) mussel density ρ_M (with $d_{50}/h = 0.13$, $VR = 0.5$, $h/H = 0.48$), (b) bed roughness d_{50}/h (for three values of mussel density, $VR = 0.5$ and $h/H = 0.48$), (c) exhaling velocity ratio VR (for two values of mussel density, $d_{50}/h = 0.13$ and $h/H = 0.48$), (d) burial level h/H (for two values of bed roughness, $\rho_M = 100$ mussels/m² and $VR = 0.5$).

3.3. Turbulent Kinetic Energy

The presence of isolated mussels over a smooth or a gravel bed is known to result in the amplification of the *TKE* behind the shell and in vicinity of the excurrent jet in case for cases with active filtering (Lazzarin, Constantinescu, et al., 2023; Wu et al., 2020). Such *TKE* increases are also observed in the present study in the simulations conducted with relatively low values of the mussel bed density (e.g., $\rho_M \leq 200$ mussels/m²).

Longitudinal profiles of the *TKE* in the $z/H \leq 2$ region are shown in Figure 9. In the case of a gravel bed with no mussels, the main regions where the *TKE* increases are located downstream of the largest roughness elements (e.g., at $x/H = 8.25$ and $x/H = 11.75$ in Figure 9a). In the simulations conducted with $\rho_M \leq 100$ mussels/m², the *TKE* distribution near most shells is similar to that observed for an isolated mussel with same h/H and VR (Lazzarin, Constantinescu, et al., 2023), with the *TKE* peaking at the exhaling siphons and in the near wake (e.g.,

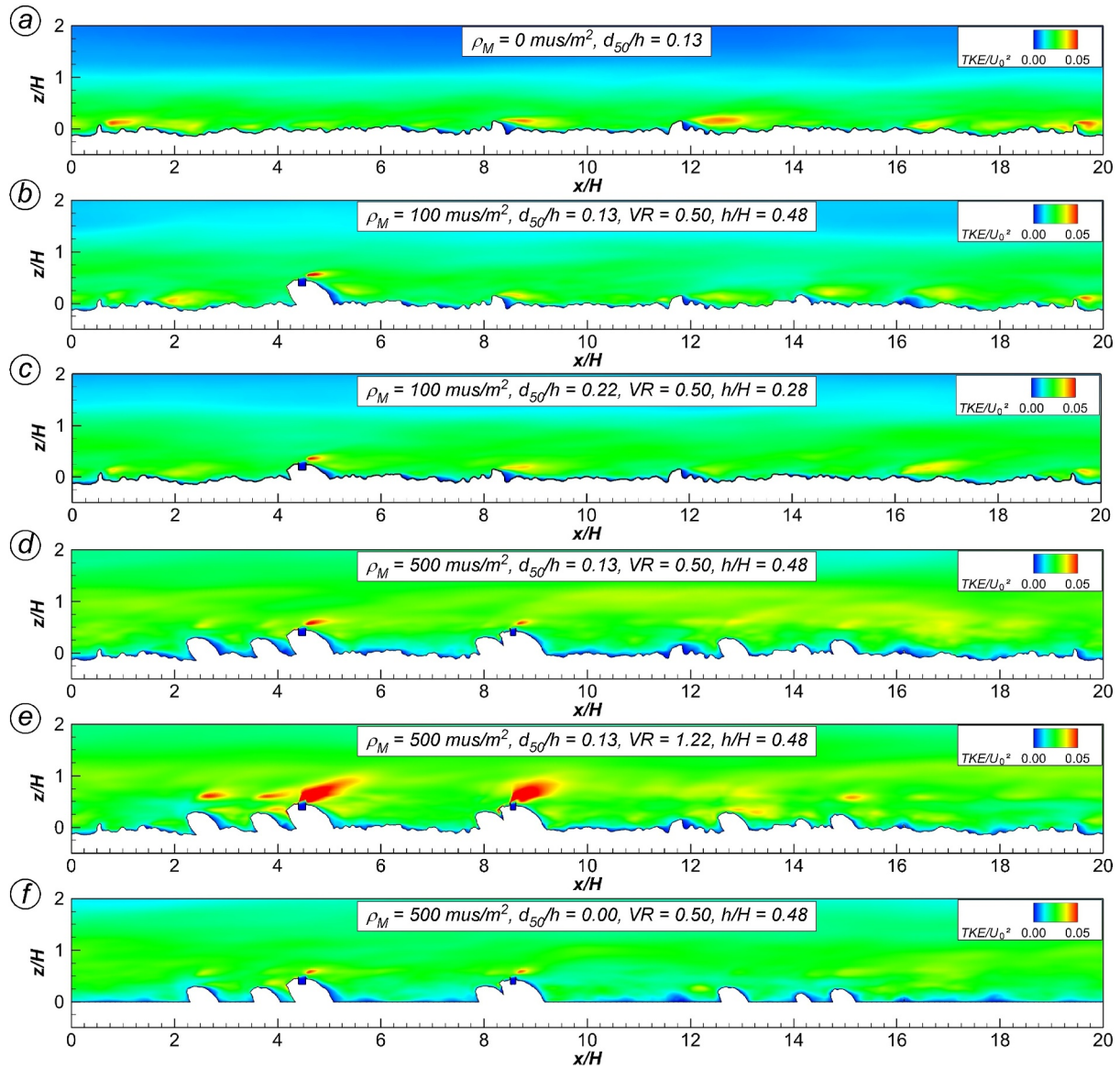


Figure 9. Turbulent kinetic energy, TKE/U_0^2 , in the $y/H = -0.7$ plane for different simulations (a–f).

see mussel at $x/H = 4.25$ in Figure 9b). As the burial level increases, the TKE in the near wake decreases (see Figure 9c), as also observed for an isolated mussel.

For very high values of the mussel bed density where wake-to-mussel interactions are very strong (e.g., for cases with $\rho_M = 500$ mussels/m²), the regions of high TKE generated by the shells extend over a larger distance above the top of the mussels and the region of high TKE becomes thicker (e.g., compare TKE in Figures 9b and 9d). As the mussel bed density increases for constant h/H and VR , the TKE inside the wakes generated by the shells decreases, mainly because of the reduction of the streamwise velocity inside the roughness layer.

The active filtering largely increases the thickness of the size of the regions of high TKE (e.g., compare TKE in Figures 9d and 9e). The main regions of high TKE are mainly found near the excurrent siphons, downstream of the top of the mussels and are penetrating way above the top of the mussels (i.e., at $z/H \approx 0.5$) due to the large vertical momentum of the excurrent jet flow. Some of regions of relatively high TKE behind the mussels in Figure 9e are generated by the interactions of the siphon-driven coherent structures with the mussel shells. The others are associated with the separated shear layer on top of the mussel.

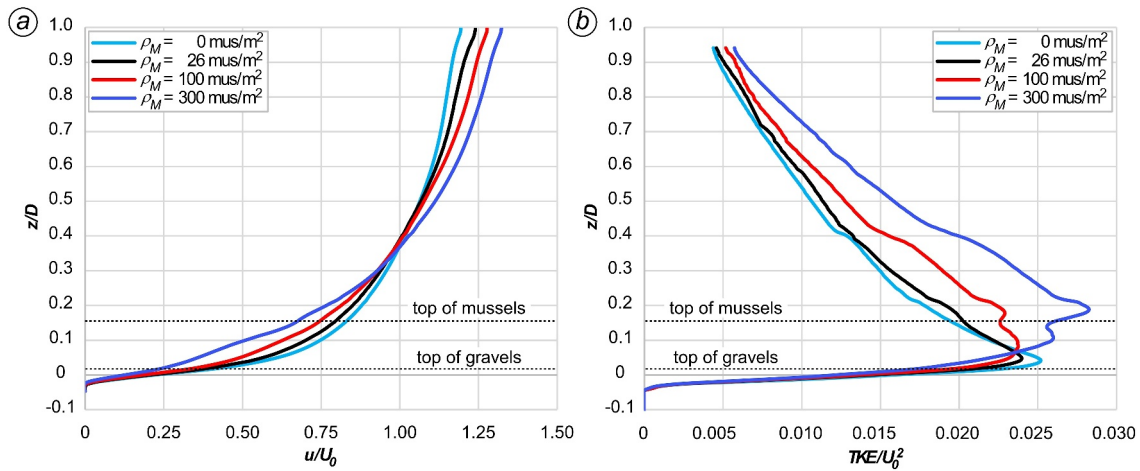


Figure 10. Vertical profiles of the double-averaged streamwise velocity (a) and turbulent kinetic energy (b) as a function of the mussel bed density ρ_M in the simulations conducted with $d_{50}/h = 0.13$, $VR = 0.5$, and $h/H = 0.48$.

As expected, for same ρ_M , VR and h/H , the TKE inside the roughness layer and some distance above it increases with increasing bed roughness (e.g., compare Figures 9d and 9f) due to the turbulence generated by the roughness elements and the additional stretching associated with interactions between eddies generated by the mussels and eddies generated by the bed roughness elements. This effect decreases with increasing mussel bed density.

To assess in a more quantitative way the effect of the mussel bed density on the mean velocity and TKE , we computed the double-averaged (e.g., width and length averaged) nondimensional profiles of these mean flow variables for some of the simulations conducted with $d_{50}/h = 0.13$, $VR = 0.5$, and $h/H = 0.48$. As expected, the presence of the shells reduces the velocity close to the bed (Figure 10a). When increasing the mussel bed density, the streamwise velocity decreases in the $0 < z < 0.35 D$ region because of the drag associated with the mussels, while it increases in the $0.35 D < z < D$ region, because of continuity. Interestingly, all velocity profiles for simulations with $h/H = 0.48$ and $d_{50}/h = 0.13$ show roughly the same velocity value at $z = 0.35 D$ (Figure 10a), which roughly corresponds to twice the exposed height of the mussel, h .

Figure 10b compares the nondimensional double-averaged TKE profiles for the same simulations of Figure 10a. In the simulation with no mussels, the TKE profiles contains a single peak at $z/D \approx 0.02$ induced by the eddies generated by the gravels. The single peak remains also in the simulation conducted with $\rho_M = 26$ mussels/m². For higher mussel density, an important qualitative change occurs as the TKE profiles display a two-peak shape. The second peak is located just above the top of the mussels (at $z/D = 0.18$) and is induced by the energetic eddies shed in the separated shear layer, especially near the top of each shell. While the TKE values for the two peaks are comparable for $\rho_M = 100$ mussels/m², the TKE peak value associated with the shells becomes larger than the TKE peak value associated with the gravels in the $\rho_M = 300$ mussels/m² simulation. With increasing mussel bed density, the gravel induced peak moves upwards, which is consistent with the reduction of TKE close to the bed for high ρ_M . The double-averaged profiles of the Reynolds shear stress (not reported here) show a behavior similar to that of the TKE . A single near-bed peak is observed for low mussel bed densities. As ρ_M increases above 100 mussels/m², the gravel-induced peak decays, and a second peak forms slightly above the top of the mussels with the corresponding TKE increasing monotonically with ρ_M . This trend is consistent with the experimental observations of Sansom et al. (2020). This result is important as it shows that around mussel bed densities of 50 mussels/m² the presence of the mussels at the bed induces a clear effect or signature on the flow structure as the large-scale eddies generated by the mussels start having a significant effect on the turbulence statistics. The profiles of the turbulence variables start diverging from the classical profiles associated with a rough-bed boundary layer or a fully developed open channel flow over a rough bed with uniform roughness.

4. Drag Forces

The protruding part of the mussels induces additional drag resistance besides that associated with the smooth or the rough bed. The total drag increases with the mussel bed density. As ρ_M increases, the streamwise flow velocity

decreases in the roughness layer and increases in the outer region (see e.g., Figure 10a), following the same trend noticed by Sansom et al. (2020).

For mussels partially burrowed within the gravels, the stability of the mussels is, to a large degree, determined by the magnitude of the drag forces acting on the emerged part of each shell (Dey, 2003; Diedericks et al., 2018; Witman & Suchanek, 1984). Lift forces are not included in the present study as they play a minor role in such cases and their estimation would require modeling the hyporheic flow within the layers of gravels to evaluate the pressure over the lower part of the shell. Modeling the flow around the gravels and the burrowed parts of the shells is beyond the scope of the present study.

Figure 11 shows the mean drag forces along the streamwise (F_{dx}^{MEAN} , blue symbols) and the spanwise (F_{dy}^{MEAN} , red symbols) directions for the different simulations listed in Table 1. Drag forces have been calculated by integrating the mean pressure acting on the emerged part of the shell. All the values are non-dimensionalized using the water density, ρ , the section-averaged flow velocity, U_0 , and the height of the mussel, H , which are constant for all simulations. Besides the mean values (filled symbols), the RMS fluctuations are also reported (empty symbols) to characterize the temporal variations with respect to the mean value. All the values reported in Figure 11 (both mean and RMS fluctuations) are averaged values for the whole mussel bed.

In the case of a low-density cluster of mussels (i.e., $\rho_M \leq 26$ mussels/m²), the value of the mean drag force in the streamwise direction, F_{dx}^{MEAN} , is close to the value predicted for an isolated mollusc by Lazzarin, Constantinescu, et al. (2023). Results also show that F_{dx}^{MEAN} decreases with increasing ρ_M (Figure 11a). The average RMS fluctuations are fairly independent of the mussel bed density and can be as high as 63% of the mean drag force for the $\rho_M = 500$ mussels/m² simulations. The mean values of the spanwise drag force and its RMS fluctuations are almost independent of ρ_M . One should note that the spanwise averaged RMS fluctuations are nearly 3 times higher than both the mean values in the spanwise direction and the RMS fluctuations in the streamwise direction. Such high mean fluctuating values can significantly reduce the stability of the partially burrowed mussels.

For a fixed value of the mussel bed density, the bed roughness has a very limited influence on the mean drag forces (Figure 11b). While F_{dy}^{MEAN} values are little influenced by bed roughness, a small decrease of F_{dx}^{MEAN} is observed with increasing roughness. The average RMS fluctuations, both in x - and in y -directions, slightly increase with increasing bed roughness, probably due to the additional turbulence induced by the gravel bed.

When increasing the filtering velocity ratio, VR , the mean streamwise force, F_{dx}^{MEAN} , decreases (Figure 11c). In particular, the rate of decrease is higher for high values of VR , in agreement to what was observed by Lazzarin, Constantinescu, et al. (2023). This may indicate that mussels may increase their filtering to reduce longitudinal forces on the shells and have a better chance to avoid dislocation from the substrate at high flow conditions. The spanwise force, F_{dy}^{MEAN} , slightly increases when increasing VR . The RMS fluctuations of the drag forces in the two directions are fairly independent of VR .

Not surprisingly, the nondimensional streamwise drag forces and the associated RMS fluctuations decrease with decreasing h/H (Figure 11d). At least for cases with $h/H = 0.48$, the bed roughness has a small effect on the rates of increase of the nondimensional streamwise drag forces with the burial level, h/H . The same trend is observed for the transverse direction.

The mean drag coefficient in the streamwise direction, for each mussel of the array, is defined as $C_{dx}^{MEAN,i} = 2F_{dx}^{MEAN,i}/(\rho U_0^2 A_x^i)$, where $F_{dx}^{MEAN,i}$ is the mean drag force in the streamwise direction for the i th mussel and A_x^i is the projected area of the emerged part of its shell. One should note that when a rough bed is considered, the projected area depends on the topography around each single mussel. The value of the mean drag coefficient for the whole array, C_{dx}^{MEAN} , follows the same trend observed for F_{dx}^{MEAN} , that is, it strongly decreases with increasing ρ_M and it slightly decreases when increasing d_{50}/h or VR (Figure 12, filled symbols in left frames); C_{dx}^{MEAN} decreases as h/H decreases from 0.48 to 0.28 mainly because the shape of the top part of the shells is more streamlined (Figure 12d). The average RMS fluctuations of the drag coefficient, C_{dx}^{RMS} , are basically independent of the aforementioned variables (Figure 12, open symbols in left frames).

Considering that the streamwise velocity in the lower part of the water column is generally reduced by the presence of increasingly denser mussel clusters, we computed the mean value of the streamwise velocity in the $z < h$ region, U_{inner} (Table 1). U_{inner} decreases with increasing ρ_M , whereas it is roughly constant when varying d_{50}/h or VR . The streamwise drag coefficient, C_{dx}^* , has been computed by replacing U_0 with U_{inner} , thus

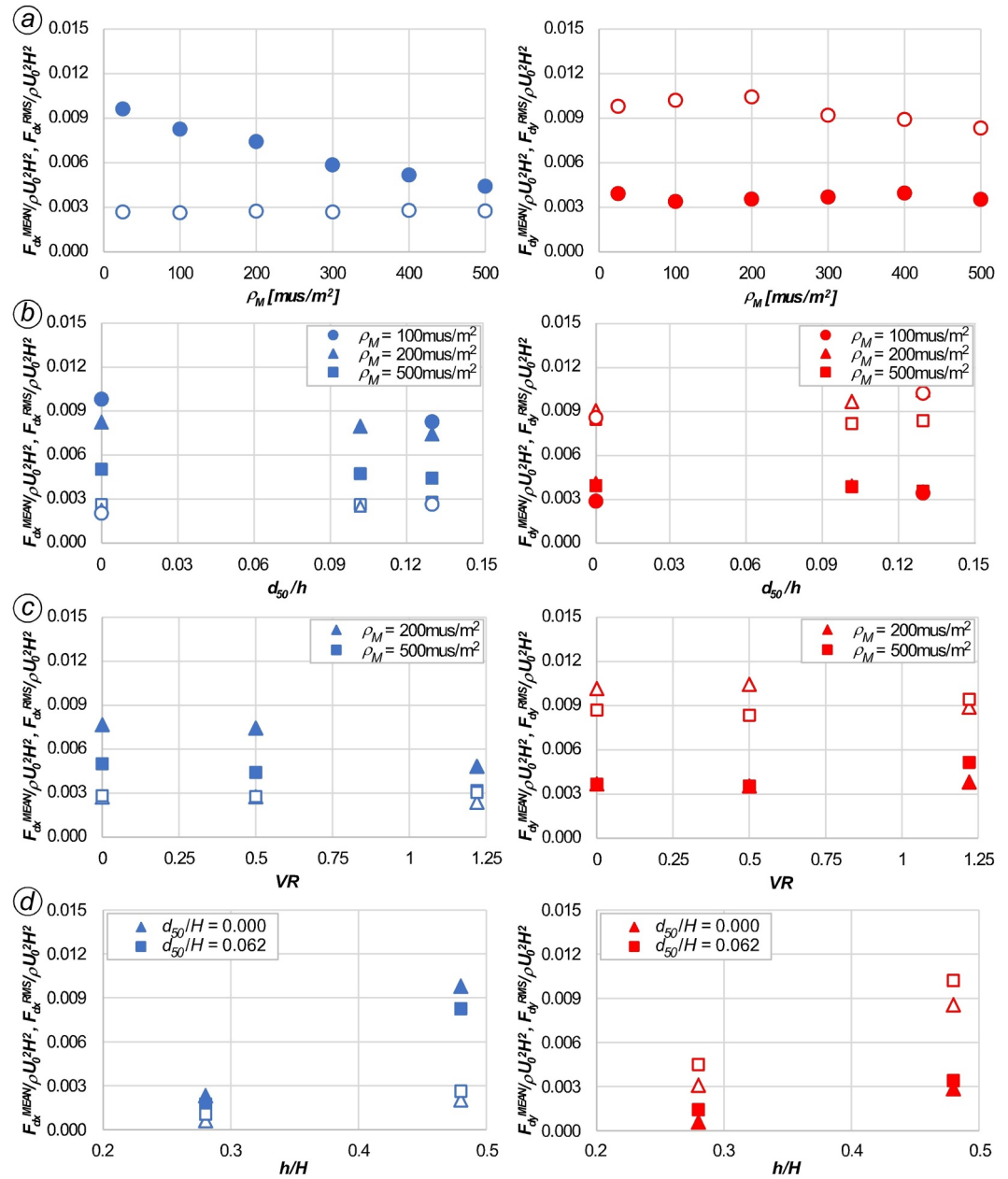


Figure 11. Mean (filled symbols) and RMS fluctuations (empty symbols) of non-dimensional mean drag forces (blue symbols refer to the x -direction, left; red symbols to the y -direction, right) as a function of (a) mussel density ρ_M (with $d_{50}/h = 0.13$, $VR = 0.5$, $h/H = 0.48$), (b) bed roughness d_{50}/h (for three values of mussel density, $VR = 0.5$ and $h/H = 0.48$), (c) exhaling velocity ratio VR (for two values of mussel density, $d_{50}/h = 0.13$ and $h/H = 0.48$), (d) burial level h/H (for two values of bed roughness, $\rho_M = 100$ mussels/m² and $VR = 0.5$).

considering the physical mean velocity approaching the shells. C_{dx}^{*MEAN} still decreases with increasing ρ_M , although at a lower rate if compared to the variation of C_{dx}^{MEAN} with the mussel bed density (Figure 12a, filled symbols). Meanwhile, C_{dx}^{*RMS} increases with increasing ρ_M (Figure 12a, empty symbols). When changing d_{50}/h , VR or h/H , C_{dx}^{*MEAN} and C_{dx}^{*RMS} exhibit the same trends as C_{dx}^{MEAN} and C_{dx}^{RMS} (Figures 12b–12d).

The values of the forces and of drag coefficients shown in Figures 11 and 12, respectively, are averaged values for the whole mussel bed. However, strong variations of the forces are observed for the various mussels, as a function of their position in the array and of their relative sheltering. These variations of the drag forces correlate with strong spatial variations of the pressure fields on the mussels (see e.g., Figure 4).

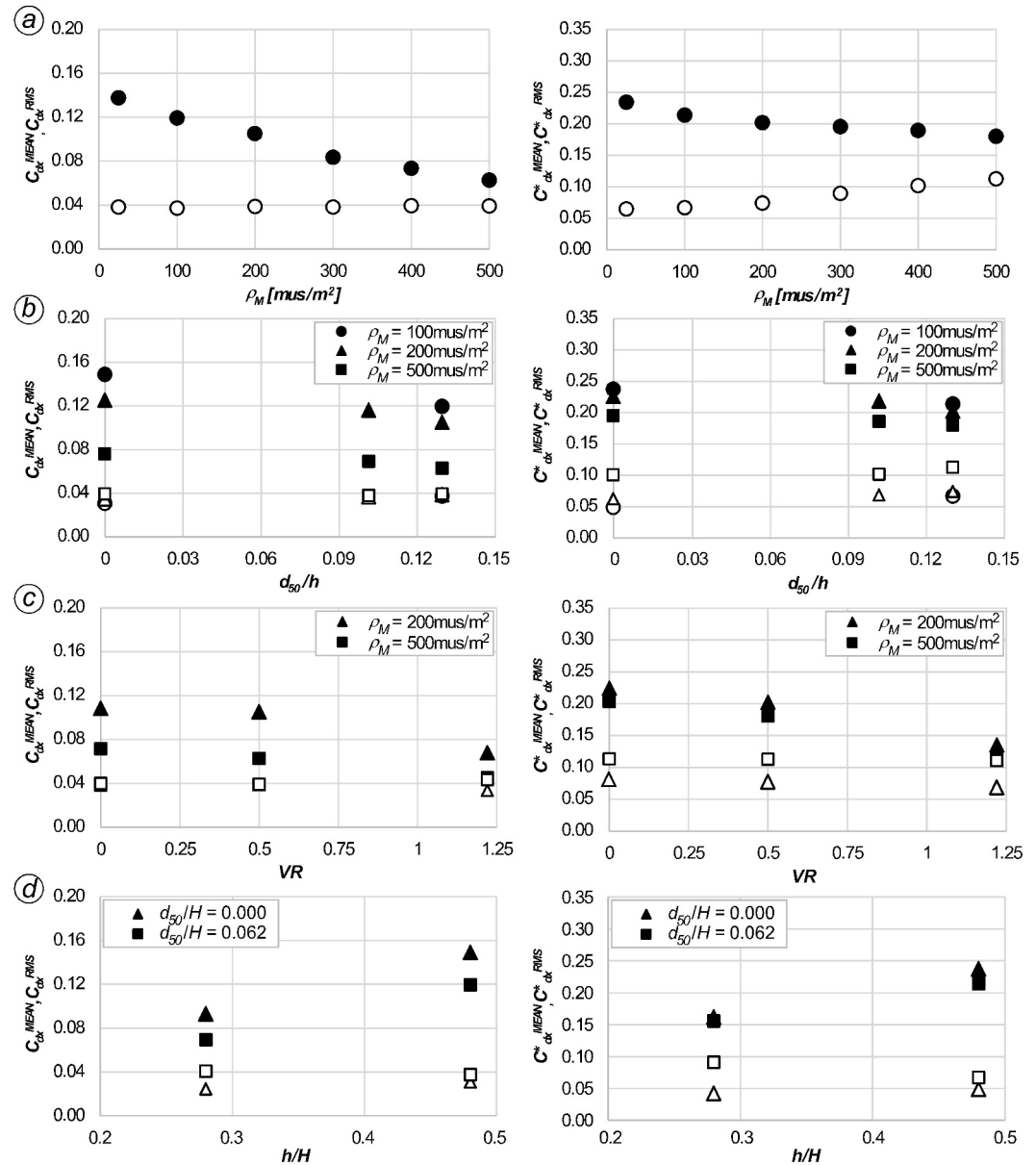


Figure 12. Mean (filled symbols) and RMS fluctuations (empty symbols) of the drag coefficient in the x -direction considering the mean velocity in the entire (C_{dx} , left) or in the inner region (C_{dx}^* , right), as a function of (a) mussel density ρ_M (with $d_{50}/h = 0.13$, $VR = 0.5$, $h/H = 0.48$), (b) bed roughness d_{50}/h (for three values of mussel density, $VR = 0.5$ and $h/H = 0.48$), (c) exhaling velocity ratio VR (for two values of mussel density, $d_{50}/h = 0.13$ and $h/H = 0.48$), (d) burial level h/H (for two values of bed roughness, $\rho_M = 100$ mussels/m² and $VR = 0.5$).

Figure 13 describes the variability of the time-averaged drag coefficient in the x -direction, $C_{dx}^{MEAN,i}$, for four cases. It compares results for smooth (frames a,c) and rough (frames b,d) bed cases and results for a sparse (100 mussels/m², frames a,b) and for a dense (500 mussels/m², frames c,d) cluster of mussels. The drag coefficients for the individual mussels are grouped in bins and results are plotted in the form of a histogram showing the distribution of the drag coefficients for the mussels forming the cluster. For dense clusters, the histogram's shape is close to that of a Gaussian (symmetrical) distribution. For sparse clusters, the distribution is more irregular. The standard deviation increases with the mussel bed density and slightly decreases in the cases with a rough bed compared to the corresponding smooth-bed cases. In the case of dense cluster ($\rho_m = 500$ mussels/m²) and smooth bed (Figure 13c), $C_{dx}^{MEAN,i}$ ranges from 0.00 to 0.20. The larger variability observed for denser clusters is due to the increased mussel-to-mussel interactions, which produce an increased sheltering for some of the mussels

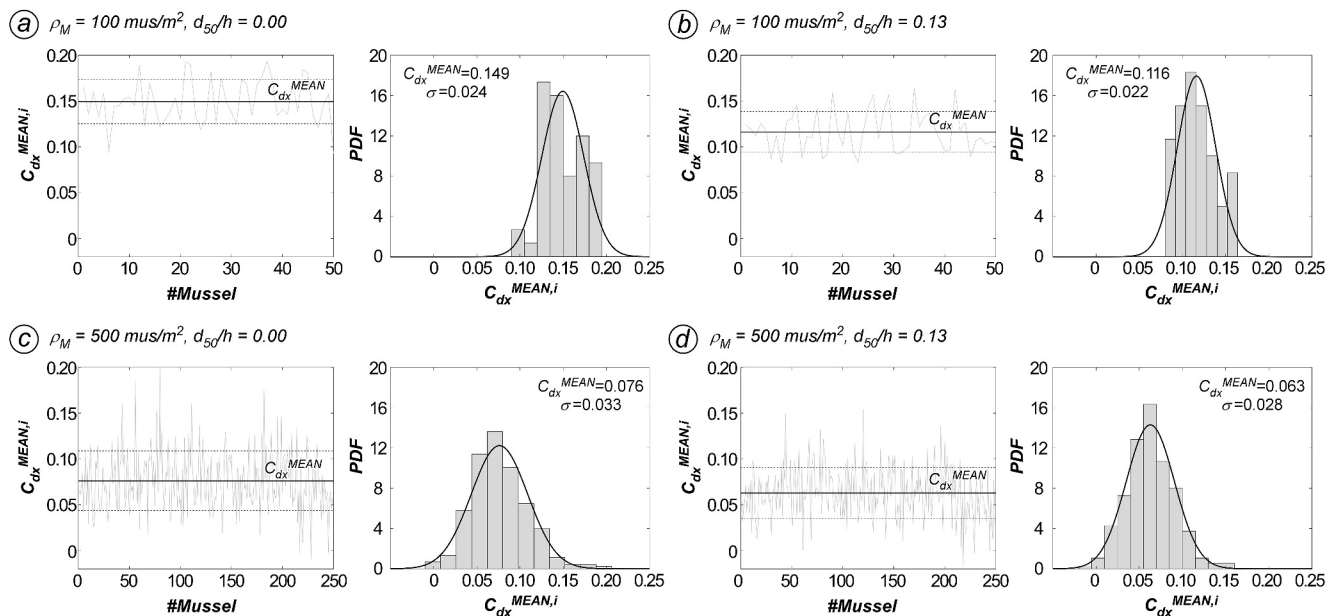


Figure 13. Streamwise (time-averaged) drag coefficients for the individual mussels forming the mussel bed for different simulations (a–d) with $VR = 0.5$ and $h/H = 0.48$. Also shown are the mean (cluster averaged) value and RMS fluctuations for the mussels in the cluster (left), the histogram of the drag coefficient for the mussels forming the cluster and comparison with the normal distribution (right).

forming the clusters. Indeed, when increasing the mussel density from 100 mussels/m² to 500 mussels/m² (see Figure 13), the maximum values of the drag coefficients remain almost the same, but the distribution shifts to the left, indicating that there is an increased number of mussels that experience a reduced drag compared to the sparser cluster. Increasing the bed roughness reduces the drag on the most exposed (i.e., less sheltered) mussels, thus reducing both the average drag and the standard deviation.

Though averaged values of the mean drag forces can be used to characterize the global effect of the flow on the mussel shells, these values do not offer a full characterization of the capacity of the individual mussels to resist dislocation from the substrate. Rather, the stability of each mussel in the array is controlled by the (maximum) instantaneous forces acting on its shell. DES simulations showed that these forces can be much higher than the cluster- and time-averaged values of drag forces because of (a) a more exposed position within the array (i.e., mean force on the individual shell is significantly higher than the average value for the whole array), and (b) instantaneous large peaks induced by high RMS fluctuations on top of the mean drag value.

5. Bed Shear Stresses

Local scour in the vicinity of the protruding part of each shell is another factor influencing mussel stability, since the increased area exposed to the flow as a result of local scour increases the drag forces on the shell that, along with a reduced anchoring within the bed, increase the probability of mussel dislocation.

In the case of gravel beds, particles entrainment is mostly driven by pressure forces acting on them. Their correct estimation requires accounting for the hyporheic flow (e.g., Fang et al., 2018; Lian et al., 2019; Rosti et al., 2018) which is beyond the scope of the present study. However, for the case of a flat bed (e.g., flat bed containing a layer of fine sand), the entrainment of bed particles is controlled by the shear stress acting on the exposed part of the channel bottom. Mean bed shear stress magnitude has been recognized to be among the key parameters controlling mussel abundance in natural streams (Daraio et al., 2010; French & Ackerman, 2014; Layzer & Madison, 1995). Thus, in cases with a flat bed, the effect of the presence of protruding shells on bed entrainment can be investigated based on the bed shear stress distributions in mean and instantaneous flow (Cheng & Constantinescu, 2022; Cheng et al., 2018; Koken et al., 2013).

Figure 14 shows the instantaneous and the mean distributions of the bed shear stresses for different mussel densities in the flat (smooth) bed simulations, scaled by the mean bed shear stress without mussels, τ_0 . Regions of

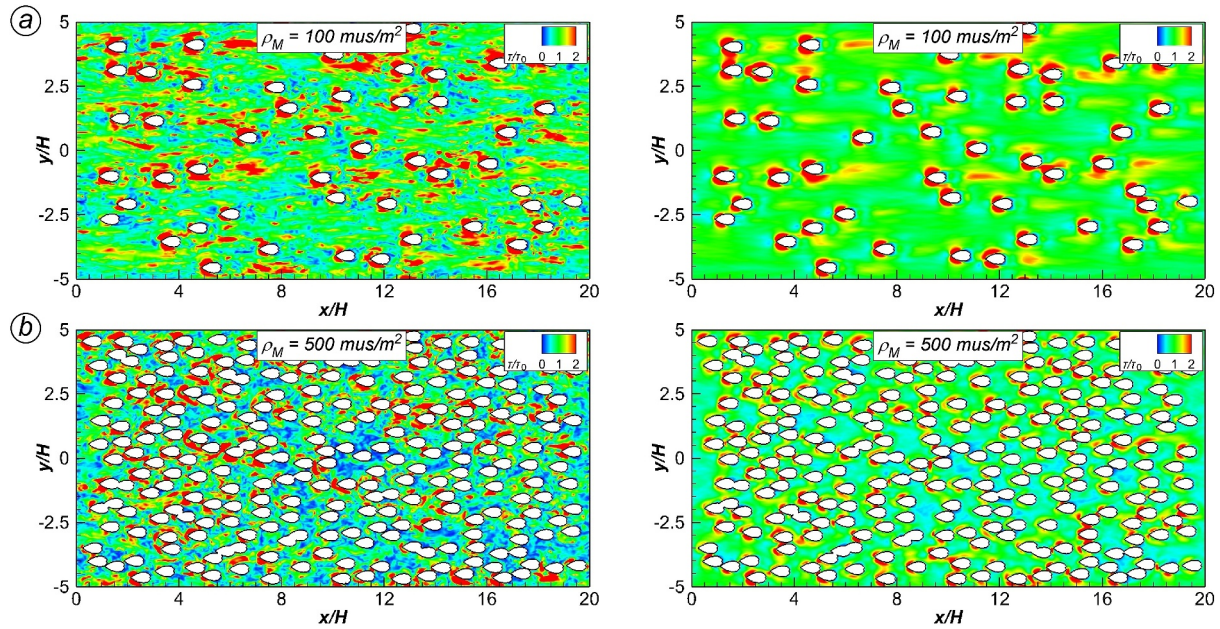


Figure 14. Instantaneous (left frame) and mean (right frame) bed shear stress, τ/τ_0 , for the simulations with $d_{50}/h = 0.000$, $VR = 0.5$, $h/H = 0.48$ and with $\rho_M = 100$ mussels/m² (a) and $\rho_M = 500$ mussels/m² (b).

high bed shear stress are observed especially at the side of mussels because of the flow acceleration. Other regions of high bed shear stress are observed downstream of the mussels, at a distance of about $2H$ from the center of the shell, where the flow reattaches to the bottom. For $\rho_M = 100$ mussels/m², the former regions are visible for all mussels; the latter regions, instead, are visible only if the downstream neighboring mussels are sufficiently spaced to allow the flow to reattach. For $\rho_M = 500$ mussels/m², both these regions are strongly reduced, and only small regions of high shear stresses are observed at the sides of the mussels.

To obtain an overall picture of the bed shear stresses with varying mussel density for the flat bed cases, one can calculate the spatially averaged mean bed shear stress over the net bed area (i.e., the portion of the bed without the part covered by the shells). Table 2 presents the values of the non-dimensional spatially averaged mean bed shear stress, $\tau^{MEAN}/(\rho U_0^2)$, for the simulations conducted with a flat bed. One can see that τ^{MEAN} increases with the mussel bed density from 100 to 200 mussels/m². The initial increase of τ^{MEAN} with ρ_M is due to the flow acceleration generated around each shell. If the mussel bed density is not very high, each mussel generates a region of high bed shear stress on its sides while the stress magnitude remains nearly independent of the mussel bed density. Results in Table 2 also show that τ^{MEAN} is smaller for 500 mussels/m² compared to 200 mussels/m² and one expects τ^{MEAN} will continue to decrease with increasing ρ_M for very large mussel bed densities. This is because of the strong decay of the momentum inside the roughness layer for high mussel bed densities when the mussels become very close to each other. More specifically, τ^{MEAN} decreases for very high mussel bed densities

mainly because of the decay of the bed shear stresses at the sides of the mussels (Figure 14). When mussels are very close to each other, regions of high shear stress are rarely forming at both sides of each mussel (Figure 14) and a number of mussels are surrounded by regions with $\tau/\tau_0 < 1$.

Interestingly, τ^{MEAN} for 500 mussels/m² is also smaller than the corresponding value for a flat bed without mussels, which shows that closely packed mussels can strongly reduce the mean streamwise velocity near the bed surface and thus “protect” the bed particles from being entrained. Given that the adverse pressure gradients and the flow acceleration around shells that are protruding less above the bed surface are lower compared to shells with a lower level of burrowing, it is not surprising that for constant mussel bed density and VR , $\tau^{MEAN}/(\rho U_0^2)$ decreases with decreasing h/H (Table 2).

Table 2

Non-Dimensional, Spatially Averaged Mean Bed Shear Stress Over the Net Bed Area, $\tau^{MEAN}/(\rho U_0^2)$

N	ρ_M	h/H	$\tau^{MEAN}/(\rho U_0^2)$
0	0	0.48	0.002361
50	100	0.48	0.002529
100	200	0.48	0.002566
250	500	0.48	0.002262
50	100	0.28	0.002124

Note. Results are shown for simulations conducted with $d_{50}/h = 0$ and $VR = 0.5$.

Overall these results show that high-density clusters of mussels have a stabilizing effect on the river bed. Given the reduced values of drag forces and bed shear stresses, dense mussel beds are expected to be favorable habitat for the mussels.

6. Summary and Conclusions

The present study investigated open channel flow over a mussel bed consisting of a large cluster of partially burrowed freshwater mussels placed on a rough or a smooth bed surface based on results of eddy-resolving numerical simulations. The present study focused on the fully developed flow regime observed at large distances from the leading edge of a long mussel bed, way downstream of the location where the internal boundary layer induced by the mussels reaches the free surface.

Simulation results showed that the increasing mussel bed density for constant level of mussel burrowing has notable consequences on the flow field and turbulence structure. Besides the expected decrease of longitudinal velocity in the roughness layer, reducing the average distance between neighboring mussels results in a reduction of the downflow at the back of the mussels that was found to have a strong effect on the bed shear stress distributions for the limiting case of isolated mussels (Lazzarin, Constantinescu, et al., 2023). The dynamics of turbulent vortices were also influenced by the mussel bed density. Moreover, results showed that for a given value of the mussel burrowing and bed roughness, there is a threshold value of the mussel bed density above which the contribution of the mussel-induced turbulence becomes dominant. This value can be determined by examining the double-averaged profiles of the turbulence statistics that start displaying a second peak once the mussel-induced turbulence becomes dominant. For example, a threshold value of around 50 mussels/m² was determined for $d_{50}/h = 0.13$, $VR = 0.5$, and $h/H = 0.48$. While the dynamics and mixing of the excurrent siphon jets were qualitatively similar to those observed for an isolated mussel, the tip vortices forming at the back of the shells were strongly dampened with increasing ρ_M due to the presence of other shells. While the effect of bed roughness was found to be significant for sparse clusters, it progressively became less important with increasing ρ_M mostly because the near-bed flow is controlled more and more by the roughness associated with the protruding shells while the roughness associated with the bed particles hardly affects the near-bed flow for the largest mussel bed densities considered in the present study.

As expected, increasing mussel density for constant mussel burrowing level reduces the average values of the mean drag force acting on the protruding mussel shells, which is beneficial for the stability of mussels. However, present results showed that the drag forces acting on the individual mussels forming the array were subject to large variations with respect to the predicted mean drag coefficient for the mussel bed. The drag coefficient for the individual mussels was found to depend on the mussel position inside the array, as some of the shells were subject to mean drag forces that were up to two times larger than the array-averaged value. Simulations conducted with smooth beds also showed that past a threshold value of the mussel bed density, the bed shear stresses decay with increasing ρ_M , meaning that dense clusters of mussels can help stabilizing the river bed. The aforementioned trends in the variation of the drag forces and of the bed shear stresses allow us to conclude that sufficiently dense clusters of mussels favor bed and mussel stability and conservation. Present results also showed that the streamwise drag force and the associated drag coefficient decrease fairly significantly with increasing filtering discharge for sufficiently high exhaling velocity ratios. So, mussels can theoretically increase their filtering activity to avoid dislocation from the substrate. The present study conducted for mussels aligned with the mean flow in the channel also showed that spanwise drag forces and the associated fluctuations can be significant especially for large mussel bed densities. This is because the local mean incoming flow is not necessarily aligned with the major axis of each mussel inside the array and because the two valves are not identical. For mussel densities close to 500 mussels/m², results showed that the mean streamwise and spanwise drag forces become comparable, while the RMS fluctuations of the drag force are larger along the spanwise direction. Both the averaged values of the spanwise drag force and its RMS fluctuations were found to be fairly independent of ρ_M , bed roughness and filtering activity for constant h/H . This may make it easier to model the spanwise drag forces and their effects on mussel stability.

Values of the drag coefficients obtained from the present simulations can be used in reduced-order models to approximate the drag coefficient value in the extra drag terms added in the momentum equations inside the roughness layer that is formally treated as a porous layer. Such a simplified (momentum-forcing) approach based on either RANS or LES is computationally much less expensive compared to the present approach, as the flow

around the shells is not resolved, similarly to what is commonly used to model the presence of vegetation in natural river reaches (e.g., Etminan et al., 2017; Kim & Stoesser, 2011). Such simplified models can be used to account for the presence of mussels at the river bed in practical applications that require simulating flow in very long river reaches.

The results of this work are also useful to explain some of the mechanisms that control the arrangement of mussels within the array, such as the formation of dense aggregations in most rivers where mussels survive over very long periods. Simulations results suggest that the formation of dense arrays is favored by the reduced drag forces and bed shear stresses compared to isolated shells and low-density clusters. This is a main reason why dense mussel beds tend to be common in rivers, though unsteady flows (such as flood or drought events) can influence the natural arrangement of the mussels and dislocate part of the mussel bed.

The present work considered only mussel beds composed of fixed identical specimens and all oriented along the same direction, whereas in natural streams heterogeneous and dynamic conditions are observed (i.e., beds with live mussels, of different size, orientation, burrowing height, filtering activity). The present work also considered only relatively high submergence ratios and an impermeable substrate (e.g., the hyporheic flow was neglected). Further research on these topics is needed to investigate how the flow physics changes for more complex cases and if simplified models can be proposed to estimate the mean drag forces acting on the shells forming the mussel bed, as well as the forces acting on the individual mussels forming the array. Experimental studies are also needed to estimate whether, or not, mussel dislocation will occur given a certain value of the streamwise and spanwise drag forces acting on the mussel, the shape of the shell, which depends on the mussel species, and the substrate characteristics. Such information is critical to be able to numerically predict how the occurrence of a certain set of flow conditions in the river reach, typically associated with flooding conditions, can affect the stability of the mussel bed.

Data Availability Statement

The data can be accessed online at <https://researchdata.cab.unipd.it/922/>.

Acknowledgments

This study was supported by Italian National Research Programme PRIN 2017, with the project 2017SEB7Z8 “Interactions between hydrodynamic flows and biotic communities in fluvial ecosystems: advancement in discharge monitoring and understanding of Processes Relevant for ecosystem sustainability by the development of novel technologies with field observations and laboratory testing (ENTERPRISING).” The CINECA award HP10COF04 N under the ISCR initiative is acknowledged for the availability of high-performance computing resources and support. The authors gratefully acknowledge Prof. D. Termini from Univ. Palermo, Italy, for providing the digital reproduction of the gravel bed and the mussel shell used in the present work. Nicoletta Riccardi, permanent researcher at CNR—IRSA, is gratefully acknowledged for providing the mussel used in the experiments and valuable information on mussel anatomy and filtering activity. T. Lazzarin is sponsored by a PhD scholarship funded by the CARIPARO Foundation, and by a scholarship provided by the A. Gini foundation for his research period at IIHR-Hydroscience and Engineering, The University of Iowa, USA. G. Constantinescu and H. Wu acknowledge partial support from the EAR Hydrologic Science Program of the US National Science Foundation under Grant 1659518.

References

- Allen, D. C., & Vaughn, C. C. (2009). Burrowing behavior of freshwater mussels in experimentally manipulated communities. *Journal of the North American Benthological Society*, 28(1), 93–100. <https://doi.org/10.1899/07-170.1>
- André, C., Jonsson, P., & Lindegarh, M. (1993). Predation on settling bivalve larvae by benthic suspension feeders: The role of hydrodynamics and larval behaviour. *Marine Ecology Progress Series*, 97, 183–192. <https://doi.org/10.3354/meps097183>
- Atkinson, C. L., & Vaughn, C. C. (2015). Biogeochemical hotspots: Temporal and spatial scaling of the impact of freshwater mussels on ecosystem function. *Freshwater Biology*, 60(3), 563–574. <https://doi.org/10.1111/fwb.12498>
- Bunt, C. M., MacIsaac, H. J., & Sprules, W. G. (1993). Pumping rates and projected filtering impacts of Juvenile Zebra mussels (*Dreissena polymorpha*) in Western Lake Erie. *Canadian Journal of Fisheries and Aquatic Sciences*, 50(5), 1017–1022. <https://doi.org/10.1139/f93-117>
- Butman, C. A., Fréchette, M., Geyer, W. R., & Starczak, V. R. (1994). Flume experiments on food supply to the blue mussel *Mytilus edulis* L. as a function of boundary-layer flow. *Limnology & Oceanography*, 39(7), 1755–1768. <https://doi.org/10.4319/lo.1994.39.7.1755>
- Chang, K., & Constantinescu, G. (2013). Coherent structures in flow over two-dimensional dunes. *Water Resources Research*, 49(5), 2446–2460. <https://doi.org/10.1002/wrcr.20239>
- Chang, W. Y., Constantinescu, G., & Tsai, W. F. (2017). On the flow and coherent structures generated by a circular array of rigid emerged cylinders placed in an open channel with flat and deformed bed. *Journal of Fluid Mechanics*, 831, 1–40. <https://doi.org/10.1017/jfm.2017.558>
- Chang, W.-Y., Constantinescu, G., & Tsai, W.-F. (2020). Effect of array submergence on flow and coherent structures through and around a circular array of rigid vertical cylinders. *Physics of Fluids*, 32(3), 035110. <https://doi.org/10.1063/1.5138604>
- Cheng, Z., & Constantinescu, G. (2022). Shallow mixing interfaces between parallel streams of unequal densities. *Journal of Fluid Mechanics*, 945, A2. <https://doi.org/10.1017/jfm.2022.505>
- Cheng, Z., Koken, M., & Constantinescu, G. (2018). Approximate methodology to account for effects of coherent structures on sediment entrainment in RANS simulations with a movable bed and applications to pier scour. *Advances in Water Resources*, 120, 65–82. <https://doi.org/10.1016/j.advwatres.2017.05.019>
- Coco, G., Thrush, S. F., Green, M. O., & Hewitt, J. E. (2006). Feedbacks between bivalve density, flow, and suspended sediment concentration on patch stable states. *Ecology*, 87(11), 2862–2870. [https://doi.org/10.1890/0012-9658\(2006\)87\[2862:FBBDFAJ\]2.0.CO;2](https://doi.org/10.1890/0012-9658(2006)87[2862:FBBDFAJ]2.0.CO;2)
- Constantinescu, G. (2014). LE of shallow mixing interfaces: A review. *Environmental Fluid Mechanics*, 14(5), 971–996. <https://doi.org/10.1007/s10652-013-9303-6>
- Constantinescu, G., Chapelet, M., & Squires, K. (2003). Turbulence modeling applied to flow over a sphere. *AIAA Journal*, 41(9), 1733–1742. <https://doi.org/10.2514/2.7291>
- Constantinescu, G., Miyawaki, S., & Liao, Q. (2013). Flow and turbulence structure past a cluster of freshwater mussels. *Journal of Hydraulic Engineering*, 139(4), 347–358. [https://doi.org/10.1061/\(ASCE\)HY.1943-7900.0000692](https://doi.org/10.1061/(ASCE)HY.1943-7900.0000692)
- Crimaldi, J. P., Koseff, J. R., & Monismith, S. G. (2007). Structure of mass and momentum fields over a model aggregation of benthic filter feeders. *Biogeosciences*, 4(3), 269–282. <https://doi.org/10.5194/bg-4-269-2007>
- Crimaldi, J. P., Thompson, J. K., Rosman, J. H., Lowe, R. J., & Koseff, J. R. (2002). Hydrodynamics of larval settlement: The influence of turbulent stress events at potential recruitment sites. *Limnology & Oceanography*, 47(4), 1137–1151. <https://doi.org/10.4319/lo.2002.47.4.1137>

- Daraio, J. A., Weber, L. J., & Newton, T. J. (2010). Hydrodynamic modeling of juvenile mussel dispersal in a large river: The potential effects of bed shear stress and other parameters. *Journal of the North American Benthological Society*, 29(3), 838–851. <https://doi.org/10.1899/09-118.1>
- de Jager, M., van de Koppel, J., Weerman, E. J., & Weissing, F. J. (2020). Patterning in mussel beds explained by the interplay of multi-level selection and spatial self-organization. *Frontiers in Ecology and Evolution*, 8. <https://doi.org/10.3389/fevo.2020.00007>
- Dey, S. (2003). Incipient motion of bivalve shells on sand beds under flowing water. *Journal of Engineering Mechanics*, 129(2), 232–240. [https://doi.org/10.1061/\(ASCE\)0733-9399\(2003\)129:2\(232\)](https://doi.org/10.1061/(ASCE)0733-9399(2003)129:2(232))
- Diedericks, G. P. J., Troch, C. N. A., & Smit, G. J. F. (2018). Incipient motion of shells and shell gravel. *Journal of Hydraulic Engineering*, 144(3), 06017030. [https://doi.org/10.1061/\(ASCE\)HY.1943-7900.0001421](https://doi.org/10.1061/(ASCE)HY.1943-7900.0001421)
- Di Maio, J., & Corkum, L. D. (1997). Patterns of orientation in unionids as a function of rivers with differing hydrological variability. *Journal of Molluscan Studies*, 63(4), 531–539. <https://doi.org/10.1093/mollus/63.4.531>
- Etminan, V., Lowe, R. J., & Ghisalberti, M. (2017). A new model for predicting the drag exerted by vegetation canopies. *Water Resources Research*, 53(4), 3179–3196. <https://doi.org/10.1002/2016WR020090>
- Fang, H., Han, X., He, G., & Dey, S. (2018). Influence of permeable beds on hydraulically macro-rough flow. *Journal of Fluid Mechanics*, 847, 552–590. <https://doi.org/10.1017/jfm.2018.314>
- Ferreira-Rodríguez, N., Akiyama, Y. B., Aksenoova, O. V., Araujo, R., Christopher Barnhart, M., Bepalaya, Y. V., et al. (2019). Research priorities for freshwater mussel conservation assessment. *Biological Conservation*, 231, 77–87. <https://doi.org/10.1016/j.biocon.2019.01.002>
- Folkard, A. M., & Gascoigne, J. C. (2009). Hydrodynamics of discontinuous mussel beds: Laboratory flume simulations. *Journal of Sea Research*, 62(4), 250–257. <https://doi.org/10.1016/j.seares.2009.06.001>
- French, S. K., & Ackerman, J. D. (2014). Responses of newly settled juvenile mussels to bed shear stress: Implications for dispersal. *Freshwater Science*, 33(1), 46–55. <https://doi.org/10.1086/674983>
- Froufe, E., Lopes-Lima, M., Riccardi, N., Zaccara, S., Vanetti, I., Lajtner, J., et al. (2017). Lifting the curtain on the freshwater mussel diversity of the Italian Peninsula and Croatian Adriatic coast. *Biodiversity & Conservation*, 26(14), 3255–3274. <https://doi.org/10.1007/s10531-017-1403-z>
- Gutiérrez, J. L., Jones, C. G., Strayer, D. L., & Iribarne, O. O. (2003). Mollusks as ecosystem engineers: The role of shell production in aquatic habitats. *Oikos*, 101(1), 79–90. <https://doi.org/10.1034/j.1600-0706.2003.12322.x>
- Hajimirzaie, S. M., Wojcik, C. J., & Buchholz, J. H. J. (2012). The role of shape and relative submergence on the structure of wakes of low-aspect-ratio wall-mounted bodies. *Experiments in Fluids*, 53(6), 1943–1962. <https://doi.org/10.1007/s00348-012-1406-1>
- Hajisafarali, M., Aaltonen, S., Pulkkinen, K., & Taskinen, J. (2022). Does the freshwater mussel *Anodonta anatina* remove the fish pathogen *Flavobacterium columnare* from water? *Hydrobiologia*, 849(4), 1067–1081. <https://doi.org/10.1007/s10750-021-04769-6>
- Heinz, S. (2020). A review of hybrid RANS-LES methods for turbulent flows: Concepts and applications. *Progress in Aerospace Sciences*, 114, 100597. <https://doi.org/10.1016/j.paerosci.2019.100597>
- Howard, J. K., & Cufey, K. M. (2006). The functional role of native freshwater mussels in the fluvial benthic environment. *Freshwater Biology*, 51(3), 460–474. <https://doi.org/10.1111/j.1365-2427.2005.01507.x>
- Keylock, C. J., Constantinescu, G., & Hardy, R. J. (2012). The application of computational fluid dynamics to natural river channels: Eddy resolving versus mean flow approaches. *Geomorphology*, 179, 1–20. <https://doi.org/10.1016/j.geomorph.2012.09.006>
- Khosronejad, A., Kang, S., & Sotiropoulos, F. (2012). Experimental and computational investigation of local scour around bridge piers. *Advances in Water Resources*, 37, 73–85. <https://doi.org/10.1016/j.advwatres.2011.09.013>
- Kim, S. J., & Stoesser, T. (2011). Closure modeling and direct simulation of vegetation drag in flow through emergent vegetation. *Water Resources Research*, 47(10). <https://doi.org/10.1029/2011WR010561>
- Koken, M., & Constantinescu, G. (2009). An investigation of the dynamics of coherent structures in a turbulent channel flow with a vertical sidewall obstruction. *Physics of Fluids*, 21(8), 085104. <https://doi.org/10.1063/1.3207859>
- Koken, M., & Constantinescu, G. (2020). Flow structure inside and around a rectangular array of rigid emerged cylinders located at the sidewall of an open channel. *Journal of Fluid Mechanics*, 910, A2. <https://doi.org/10.1017/jfm.2020.900>
- Koken, M., & Constantinescu, G. (2023). Influence of submergence ratio on flow and drag forces generated by a long rectangular array of rigid cylinders at the sidewall of an open channel. *Journal of Fluid Mechanics*, 966, A5. <https://doi.org/10.1017/jfm.2023.427>
- Koken, M., Constantinescu, G., & Blanckaert, K. (2013). Hydrodynamic processes, sediment erosion mechanisms, and Reynolds-number-induced scale effects in an open channel bend of strong curvature with flat bathymetry. *Journal of Geophysical Research: Earth Surface*, 118(4), 2308–2324. <https://doi.org/10.1002/2013JF002760>
- Kreeger, D. A., Gatenby, C. M., & Bergstrom, P. W. (2018). Restoration potential of several native species of bivalve molluscs for water quality improvement in Mid-Atlantic Watersheds. *Journal of Shellfish Research*, 37(5), 1121–1157. <https://doi.org/10.2983/035.037.0524>
- Kryger, J., & Riisgård, H. U. (1988). Filtration rate capacities in 6 species of European freshwater bivalves. *Oecologia*, 77(1), 34–38. <https://doi.org/10.1007/BF00380921>
- Kumar, S. S., Kozarek, J., Hornbach, D., Hondzo, M., & Hong, J. (2019). Experimental investigation of turbulent flow over live mussels. *Environmental Fluid Mechanics*, 19(6), 1417–1430. <https://doi.org/10.1007/s10652-019-09664-2>
- Layzer, J. B., & Madison, L. M. (1995). Microhabitat use by freshwater mussels and recommendations for determining their instream flow needs. *Regulated Rivers: Research & Management*, 10(2–4), 329–345. <https://doi.org/10.1002/rrr.3450100225>
- Lazzarin, T., Constantinescu, G., Di Micco, L., Wu, H., Lavignani, F., Lo Brutto, M., et al. (2023). Influence of bed roughness on flow and turbulence structure around a partially-buried, isolated freshwater mussel. *Water Resources Research*, 59(4), e2022WR034151. <https://doi.org/10.1029/2022WR034151>
- Lazzarin, T., Viero, D. P., Defina, A., & Cozzolino, L. (2023). Flow under vertical sluice gates: Flow stability at large gate opening and disambiguation of partial dam-break multiple solutions. *Physics of Fluids*, 35(2), 024114. <https://doi.org/10.1063/5.0131953>
- Lian, Y. P., Dallmann, J., Sonin, B., Roche, K. R., Liu, W. K., Packman, A. I., & Wagner, G. J. (2019). Large eddy simulation of turbulent flow over and through a rough permeable bed. *Computers & Fluids*, 180, 128–138. <https://doi.org/10.1016/j.compfluid.2018.12.015>
- Liu, Q.-X., Herman, P. M. J., Mooij, W. M., Huisman, J., Scheffer, M., Olf, H., & van de Koppel, J. (2014). Pattern formation at multiple spatial scales drives the resilience of mussel bed ecosystems. *Nature Communications*, 5(1), 5234. <https://doi.org/10.1038/ncomms6234>
- Lopes-Lima, M., Sousa, R., Geist, J., Aldridge, D. C., Araujo, R., Bergengren, J., et al. (2017). Conservation status of freshwater mussels in Europe: State of the art and future challenges. *Biological Reviews*, 92(1), 572–607. <https://doi.org/10.1111/bvr.12244>
- Lopez, J. W., DuBose, T. P., Franzen, A. J., Atkinson, C. L., & Vaughn, C. C. (2022). Long-term monitoring shows that drought sensitivity and riparian land use change coincide with freshwater mussel declines. *Aquatic Conservation: Marine and Freshwater Ecosystems*, 32(10), 1571–1583. <https://doi.org/10.1002/aqc.3884>
- Lopez, J. W., & Vaughn, C. C. (2021). A review and evaluation of the effects of hydrodynamic variables on freshwater mussel communities. *Freshwater Biology*, 66(9), 1665–1679. <https://doi.org/10.1111/fwb.13784>

- Marrone, F., Gianbattista, N., Cianfanelli, S., Govedic, M., Barra, S., Arculeo, M., & Bodon, M. (2019). Diversity and taxonomy of the genus *Unio* Philipsson in Italy, with the designation of a neotype for *Unio elongatulus* C. Pfeiffer (Mollusca, Bivalvia, Unionidae). *Zootaxa*, 4545(3), 339–374. <https://doi.org/10.11646/zootaxa.4545.3.2>
- Menter, F. (1994). Two-equation eddy-viscosity turbulence models for engineering applications. *AIAA Journal*, 32(8), 1598–1605. <https://doi.org/10.2514/3.12149>
- Menter, F., Hüppe, A., Matyushenko, A., & Kolmogorov, D. (2021). An overview of hybrid RANS–LES models developed for industrial CFD. *Applied Sciences*, 11(6), 2459. <https://doi.org/10.3390/app11062459>
- Menter, F., Kuntz, M., & Langtry, R. (2003). Ten years of industrial experience with the SST turbulence model. *Heat and Mass Transfer*, 625–632.
- Miller, A. C., & Payne, B. S. (1988). The need for quantitative sampling to characterize size demography and density of fresh water mussel communities. *American Malacological Bulletin*, 6(1), 49–54.
- Modesto, V., Tosato, L., Pilbala, A., Benistati, N., Fraccarollo, L., Termini, D., et al. (2023). Mussel behaviour as a tool to measure the impact of hydrodynamic stressors. *Hydrobiologia*, 850(4), 807–820. <https://doi.org/10.1007/s10750-022-05126-x>
- Monismith, S. G., Koseff, J. R., Thompson, J. K., O’Riordan, C. A., & Nepf, H. M. (1990). A study of model bivalve siphonal currents. *Limnology & Oceanography*, 35(3), 680–696. <https://doi.org/10.4319/lo.1990.35.3.0680>
- Morales, Y., Weber, L. J., Mynett, A. E., & Newton, T. J. (2006). Effects of substrate and hydrodynamic conditions on the formation of mussel beds in a large river. *Journal of the North American Benthological Society*, 25(3), 664–676. [https://doi.org/10.1899/0887-3593\(2006\)25\[664:EOSAHC\]2.0.CO;2](https://doi.org/10.1899/0887-3593(2006)25[664:EOSAHC]2.0.CO;2)
- Nikora, V. (2010). Hydrodynamics of aquatic ecosystems: An interface between ecology, biomechanics and environmental fluid mechanics. *River Research and Applications*, 26(4), 367–384. <https://doi.org/10.1002/rra.1291>
- Nikora, V., Green, M., Thrush, S., Hume, T., & Goring, D. (2002). Structure of the internal boundary layer over a patch of horse mussels (*Atrina zelandica*) in an estuary. *Journal of Marine Research*, 60(1), 121–150. <https://doi.org/10.1357/002224002762341276>
- Nishizaki, M., & Ackerman, J. D. (2017). Mussels blow rings: Jet behavior affects local mixing. *Limnology & Oceanography*, 62(1), 125–136. <https://doi.org/10.1002/lno.10380>
- O’Riordan, C. A., Monismith, S. G., & Koseff, J. R. (1995). The effect of bivalve excurrent jet dynamics on mass transfer in a benthic boundary layer. *Limnology & Oceanography*, 40(2), 330–344. <https://doi.org/10.4319/lo.1995.40.2.0330>
- Patankar, S. V., & Spalding, D. B. (1972). A calculation procedure for heat, mass and momentum transfer in three-dimensional parabolic flows. *International Journal of Heat and Mass Transfer*, 15(10), 1787–1806. [https://doi.org/10.1016/0017-9310\(72\)90054-3](https://doi.org/10.1016/0017-9310(72)90054-3)
- Perles, S. J., Christian, A. D., & Berg, D. J. (2003). Vertical migration, orientation, aggregation, and fecundity of the freshwater mussel *Lampsilis siliquoidea*. *Ohio Journal of Science*, 103(4), 73–78.
- Pilbala, A., Riccardi, N., Benistati, N., Modesto, V., Termini, D., Manca, D., et al. (2024). Real-time biological early-warning system based on freshwater mussels’ valvometry data. *Hydrology and Earth System Sciences*, 28(10), 2297–2311. <https://doi.org/10.5194/hess-28-2297-2024>
- Polvi, L. E., & Sarneel, J. M. (2018). Ecosystem engineers in rivers: An introduction to how and where organisms create positive biogeomorphic feedbacks. *WIREs Water*, 5(2), e1271. <https://doi.org/10.1002/wat2.1271>
- Riisgård, H. U., Jørgensen, B. H., Lundgreen, K., Storti, F., Walther, J. H., Meyer, K. E., & Larsen, P. S. (2011). The exhalant jet of mussels *Mytilus edulis*. *Marine Ecology Progress Series*, 437, 147–164. <https://doi.org/10.3354/meps09268>
- Rosti, M. E., Brandt, L., & Pinelli, A. (2018). Turbulent channel flow over an anisotropic porous wall – Drag increase and reduction. *Journal of Fluid Mechanics*, 842, 381–394. <https://doi.org/10.1017/jfm.2018.152>
- Sansom, B. J., Atkinson, J. F., & Bennett, S. J. (2018). Modulation of near-bed hydrodynamics by freshwater mussels in an experimental channel. *Hydrobiologia*, 810(1), 449–463. <https://doi.org/10.1007/s10750-017-3172-9>
- Sansom, B. J., Bennett, S. J., & Atkinson, J. F. (2022). Freshwater mussel burrow position and its relation to streambed roughness. *Freshwater Science*, 41(2), 315–326. <https://doi.org/10.1086/719993>
- Sansom, B. J., Bennett, S. J., Atkinson, J. F., & Vaughn, C. C. (2020). Emergent hydrodynamics and skimming flow over mussel covered beds in rivers. *Water Resources Research*, 56(8), e2019WR026252. <https://doi.org/10.1029/2019WR026252>
- Shamloo, H., Rajaratnam, N., & Katopodis, C. (2001). Hydraulics of simple habitat structures. *Journal of Hydraulic Research*, 39(4), 351–366. <https://doi.org/10.1080/00221680109499840>
- Simeone, D., Tagliaro, C. H., & Beasley, C. R. (2021). Amazonian freshwater mussel density: A useful indicator of macroinvertebrate assemblage and habitat quality. *Ecological Indicators*, 122, 107300. <https://doi.org/10.1016/j.ecolind.2020.107300>
- Steuer, J. J., Newton, T. J., & Zigler, S. J. (2008). Use of complex hydraulic variables to predict the distribution and density of unionids in a side channel of the Upper Mississippi River. *Hydrobiologia*, 610(1), 67–82. <https://doi.org/10.1007/s10750-008-9423-z>
- Strayer, D. L. (2008). *Freshwater mussel ecology: A multifactor approach to distribution and abundance*. University of California Press. <https://doi.org/10.1525/california/9780520255265.001.0001>
- Strayer, D. L., Hunter, D. C., Smith, L. C., & Borg, C. K. (1994). Distribution, abundance, and roles of freshwater clams (Bivalvia, Unionidae) in the freshwater tidal Hudson River. *Freshwater Biology*, 31(2), 239–248. <https://doi.org/10.1111/j.1365-2427.1994.tb00858.x>
- Sullivan, K. T., & Woolnough, D. A. (2021). Water depth, flow variability, and size class influence the movement behavior of freshwater mussels (Unionida) in Great Lakes river drainages. *Freshwater Science*, 40(2), 328–339. <https://doi.org/10.1086/714412>
- Termini, D., Benistati, N., Tosato, L., Pilbala, A., Modesto, V., Fraccarollo, L., et al. (2023). Identification of hydrodynamic changes in rivers by means of freshwater mussels’ behavioural response: An experimental investigation. *Ecohydrology*, e2544. <https://doi.org/10.1002/eco.2544>
- van de Koppel, J., Gascoigne, J. C., Theraulaz, G., Rietkerk, M., Mooij, W. M., & Herman, P. M. J. (2008). Experimental evidence for spatial self-organization and its emergent effects in mussel bed ecosystems. *Science*, 322(5902), 739–742. <https://doi.org/10.1126/science.1163952>
- van Duren, L. A., Herman, P. M. J., Sandee, A. J. J., & Heip, C. H. R. (2006). Effects of mussel filtering activity on boundary layer structure. *Exchange Processes at the Sediment-Water Interface*, 55(1), 3–14. <https://doi.org/10.1016/j.seares.2005.08.001>
- Vaughn, C. C. (2018). Ecosystem services provided by freshwater mussels. *Hydrobiologia*, 810(1), 15–27. <https://doi.org/10.1007/s10750-017-3139-x>
- Vaughn, C. C., Gido, K. B., & Spooner, D. E. (2004). Ecosystem processes performed by unionid mussels in stream mesocosms: Species roles and effects of abundance. *Hydrobiologia*, 527(1), 35–47. <https://doi.org/10.1023/B:HYDR.0000043180.30420.00>
- Vaughn, C. C., Nichols, S. J., & Spooner, D. E. (2008). Community and foodweb ecology of freshwater mussels. *Journal of the North American Benthological Society*, 27(2), 409–423. <https://doi.org/10.1899/07-058.1>
- Witman, J., & Suchanek, T. (1984). Mussels in flow: Drag and dislodgement by epizoans. *Marine Ecology - Progress Series*, 16, 259–268. <https://doi.org/10.3354/meps016259>
- Wu, H., & Constantinescu, G. (2022). Effect of angle of attack on flow past a partially-burrowed, isolated freshwater mussel. *Advances in Water Resources*, 168, 104302. <https://doi.org/10.1016/j.advwatres.2022.104302>

- Wu, H., Constantinescu, G., & Zeng, J. (2020). Flow and entrainment mechanisms around a freshwater mussel aligned with the incoming flow. *Water Resources Research*, *56*(9), e2020WR027983. <https://doi.org/10.1029/2020WR027983>
- Zigler, S. J., Newton, T. J., Steuer, J. J., Bartsch, M. R., & Sauer, J. S. (2008). Importance of physical and hydraulic characteristics to unionid mussels: A retrospective analysis in a reach of large river. *Hydrobiologia*, *598*(1), 343–360. <https://doi.org/10.1007/s10750-007-9167-1>